INFLUENCE OF CONVECTION ON MICROSTRUCTURE

NAG8 - 753

Fourth Semi-annual Progress Report

15 February 1990 to 14 August 1990

CLARKSON UNIVERSITY

Potsdam, New York 13676

Principal Investigator: Dr. William R. Wilcox
                                School of Engineering and
                                Center for Advanced Materials Processing
                                (315) 268-6446 or 2336
                                fax 6438 or 3841

Post-doctoral Research Associate:

   Dr. Rubens Caram

Graduate Student Research Assistants:

   Mr. A.P. Mohanty, M.S. Candidate in Chemical Engineering
   Ms. Jayshree Seth, M.S. Candidate in Chemical Engineering

Introduction

The primary motivation for this research is to determine the cause for space processing altering the microstructure of some eutectics, especially the MnBi-Bi eutectic. Prior experimental research at Grumman and here showed that the microstructure of MnBi-Bi eutectic is twice as fine when solidified in space or in a magnetic field, is uninfluenced by interfacial temperature gradient, adjusts very quickly to changes in freezing rate, and becomes coarser when spin-up/spin-down (accelerated crucible rotation technique) is used during solidification. Theoretical work at Clarkson predicted that buoyancy driven convection on earth could not account for the two fold change in fiber spacing caused by solidification in space. However a lamellar structure with a planar interface was assumed, and the Soret effect was not included in the analysis. Experimental work at Clarkson showed that the interface is not planar; MnBi fibers project out in front of the Bi matrix on the order of one fiber diameter.

Originally four primary hypotheses were to be tested under this current grant:

A fibrous microstructure is much more sensitive to convection than a lamellar microstructure, which was assumed in our prior theoretical treatment.

An interface with one phase projecting out into the melt is much more sensitive to convection than a planar interface, which was assumed in our prior theoretical treatment.

The Soret effect is much more important in the absence of convection and has a sufficiently large influence on microstructure that its action can explain the flight results.

The microstructure is much more sensitive to convection when the composition of the bulk melt is off eutectic.

Progress

1. The revision of the manuscript entitled "Influence of Convection on Rod Spacing of Eutectics" was accepted for publication by the Journal of Crystal Growth. This manuscript was included in the last semi-annual progress report.

2. Dr. Caram determined the influence of Soret effect on fiber spacing. He found analytical solutions for temperature versus distance (assuming constant furnace temperature) and <u>average</u> concentration versus distance (assuming steady state, no convection, and semi infinite melt). The three dimensional concentration field was solved in the neighborhood of the interface. Application of a Hunt-Jackson treatment gave the change in fiber spacing caused by the Soret effect. This change turned out to be too to explain the flight results. The change was proportional to the thermal diffusion coefficient, but did not depend strongly on the Biot number or the Peclet number. A paper was written and has been submitted to the Journal of Crystal Growth. It is attached here as Appendix A.

3. Mr. Mohanty completed his M.S. thesis, which consisted of an effort to determine the Soret and diffusion coefficients for the Mn-Bi eutectic melt. Capillaries containing molten Mn-Bi eutectic were held in a vertical gradient furnace for periods ranging from hours to weeks. The resulting melts were quenched, sectioned, and Mn analyzed by atomic absorption spectroscopy.

Two strange things occurred. First, an initial separation was observed, even in the absence of a temperature gradient. This looks like sedimentation.

The second observation was that after a long period of time the Mn concentration versus distance curves all showed a slight maximum and a slight minimum in the central portion. While not pronounced, this wave was very reproducible, so it is believed to be real. The only explanation we could think of is weak convection. (Space experiments are needed.)

Dr. Caram wrote a computer program which numerically solves the mass transfer differential equation assuming constant diffusion and Soret coefficients. Mohanty ran a series of runs using an early experimental concentration profile as an initial condition to calculate later concentration profiles, assuming a reasonable value for the diffusion coefficient. By comparison with the experimental curves he obtained an estimate for the value of the Soret coefficient, although agreement of experiment and theory was poor.

Excerpts of Mr. Mohanty's thesis are attached here as Appendix B.

4. Miss Seth has developed numerical methods to solve the problem of convective effects on lamellar spacing with alternate lamellae projecting out into the melt from the other phase. She calculates numerically the two dimensional velocity field near the interface for shear flow far from the interface, uses this to calculate the concentration field, and then uses the deviation from eutectic at the interface as in Hunt and Jackson to calculate lamellar spacing. Miss Seth's methods are outlined here as Appendix C.

Plans

1. Directionally solidify MnBi-Bi eutectic in the Soviet centrifuge apparatus. Determine the influence of g level on the microstructure.

2. Complete the theoretical study of the influence of convection on microstructure of a non-planar interface.

3. Determine experimentally the influence of vibrations on the microstructure of Pb-Sn and MnBi-Bi eutectics.

4. Determine theoretically the influence of convection on the microstructure of off-eutectic mixtures using a linear velocity gradient in the melt and a planar interface.

5. Theoretically find the influence of the Soret effect on the average concentration versus distance for an off-eutectic mixture in the absence of convection.

6. Compare Mohanty's data with theoretical predictions for other values of the diffusion coefficient.

7. Complete an examination of the influence of physical properties on the reported changes in eutectic microstructure caused by solidification in space.

It is certain that we will not be able to complete all of these tasks in the remaining year of this grant, so NASA should expect a renewal proposal in the near future.

THE SORET EFFECT IN EUTECTIC SOLIDIFICATION

R. Caram[*] and W.R. Wilcox

Clarkson University, Potsdam, NY 13699-5700, USA

ABSTRACT

In eutectic growth, as the solid phases grow they reject atoms to the liquid. This results in a variation of melt composition along the solid/liquid interface. In the past, mass transfer in eutectic solidification, in the absence of convection, was considered to be governed only by the diffusion induced by compositional gradients. However, mass transfer can also be generated by a temperature gradient. This is called thermotransport, thermomigration, thermal diffusion or the Soret effect.

This paper presents a theoretical model of the influence of the Soret effect on the growth of eutectic alloys. A differential equation describing the compositional field near the interface during unidirectional solidification of a binary eutectic alloy was formulated by including the contributions of both compositional and thermal gradients in the liquid. A steady-state solution of the differential equation was obtained by applying appropriate boundary conditions and accounting for heat flow in the melt. Following that, the average interfacial composition was converted to a variation of undercooling at the interface, and consequently to microstructural parameters.

The results obtained show that thermotransport can, under certain circumstances, be a parameter of paramount importance.

[*] Permanent address: State University of Campinas, Brazil

1. INTRODUCTION

Directional solidification applied to growth of eutectic alloys is one of the most efficient techniques to produce composite materials. In-situ composites obtained by this process typically have a notable degree of thermal stability and better properties than their individual constituents. Eutectic and eutectoid growth has been the topic of several theoretical studies since it was first studied by Zener [1] and Brandt [2]. Following these basic works, the mathematical modeling of eutectic solidification was discussed many times, including the classical work of Jackson and Hunt [3].

Recently several investigators have studied the directional solidification of eutectic alloys in space. Since microgravity greatly decreases buoyancy driven convection, eutectic solidification under such conditions is expected to result in a pure diffusion-controlled growth. During experiments on directional solidification of MnBi-Bi eutectic in the space environment, the microstructure obtained was finer than when solidification was done on earth under otherwise identical conditions [4-6]. Apparently, these results were due to reduced convection in space. Theoretical work, considering a convective flow across the interface, led to the prediction that convection during solidification coarsens an eutectic microstructure by changing the composition of the interfacial liquid [7-10]. However, the results showed that natural convection on earth is not sufficient to cause the finer microstructure observed in low gravity processed samples [11].

A reasonable hypothesis for the low gravity change in eutectic microstructure involves thermal diffusion during directional solidification. The thermal diffusion phenomenon, also known as the Soret effect, is the relative separation of the constituents of a mixture while it is held in a thermal gradient in the absence of convection [12]. In a vertical column, this separation leads one of the components to migrate upward or downward, depending on the sign of the Soret coefficient. The Soret coefficient depends on temperature, pressure and concentration [13]. The separation caused by thermomigration is dissipated by convected motion of the fluid.

During the growth of a eutectic alloy, as the solid phases are formed they segregate atoms into the liquid. This segregation causes a change in the interfacial liquid composition and, thereby, determines the eutectic microstructure [3]. When thermal diffusion occurs

2

during eutectic solidification, it is expected to induces a variation in liquid composition near the freezing interface. This change may cause a significant modification in microstructure. Even a small amount of fluid convection may be sufficient to eliminate the interfacial composition change produced by the Soret effect.

The purpose of this work is to develop a mathematical model to describe the influence of the Soret effect during the growth of dilute eutectic alloys in the absence of convection.

2. MATHEMATICAL MODEL

Consider the unidirectional solidification of a molten dilute eutectic binary alloy at steady-state [14]. As the solid/liquid transformation proceeds, two solid phases are grown and the average composition of the frozen solid is the same of the liquid far from the interface, here taken to be the eutectic composition C_E.

In order to start this analysis, an interfacial mass balance, similar to the one developed by Yue [15,16], was done. According to figure 1, in the absence of convection for one dimensional behavior the liquid composition $C(z)$ is influenced by three factors:

a. Flux due to the compositional gradient:

$$J_1 = -D\frac{\partial C}{\partial z}$$ (1)

b. Flux due to the advancing solid/liquid interface:

$$J_2 = -VC$$ (2)

c. Flux due to the temperature gradient for a dilute alloy:

$$J_3 = -D'C\frac{\partial T}{\partial z}$$ (3)

3

where D' is the thermal diffusion coefficient and D is the usual molecular diffusion coefficient. Henceforth both D' and D are assumed to be constant with respect to temperature and concentration. Here V is the rate of displacement of the interface, $\partial T/\partial z$ is the temperature gradient in the liquid at the interface, $\partial C/\partial z$ is the gradient of concentration of solute in the liquid at the interface, and z is the distance into the melt from the interface.

The total flux J_T in the z direction is:

$$J_T = J_1 + J_2 + J_3 = -D\frac{\partial C}{\partial z} - VC + D'C\frac{\partial T}{\partial z} \tag{4}$$

Assuming C and T are functions of z only, a mass balance over a differential element in the liquid yields:

$$\frac{\partial C}{\partial t} = -\frac{\partial J_T}{\partial z} = D\frac{\partial^2 C}{\partial z^2} + V\frac{\partial C}{\partial z} - D'(C\frac{\partial^2 T}{\partial z^2} + \frac{\partial T}{\partial z}\frac{\partial C}{\partial z}) \tag{5}$$

Assuming that the steady-state is reached, $\partial C/\partial t = 0$ and:

$$\frac{\partial^2 C}{\partial z^2} + \frac{V}{D}\frac{\partial C}{\partial z} - \frac{D'}{D}\frac{\partial}{\partial z}(C\frac{\partial T}{\partial z}) = 0 \tag{6}$$

If the composition varies parallel to the interface as well as normal to the interface, we have similarly in three-dimensions:

$$\nabla^2 C + \frac{V}{D}\frac{\partial C}{\partial z} - \frac{D'}{D}\frac{\partial}{\partial z}(C\frac{\partial T}{\partial z}) = 0 \tag{7}$$

In order to know the thermal diffusion we must determine the temperature profile in the melt. This can be done analytically for a thin rod in the absence of convection. Assuming the temperature is function of z only, a steady-state heat balance over a differential element gives:

$$kR\frac{\partial^2 T}{\partial z^2} + \rho C_P VR\frac{\partial T}{\partial z} + 2h(T_h - T) = 0 \tag{8}$$

4

where k is the thermal conductivity of the melt, R is the radius of the sample, ρ is its density, C_P is the heat capacity, h is the heat transfer coefficient between the rod and the heater, and T_h is the temperature of the heater. This approach is valid for $hR/k < <1$ and $k/C_P\mu < <1$, where μ is the viscosity of the melt. We non-dimensionalize by assuming T_h is constant and letting $B = hR/k$, $Pe = \rho C_P VR/k$, $\eta = z/R$ and $\Phi = (T-T_h)/(T_0-T_h)$. Then, equation 8 can be written as:

$$\frac{\partial^2\phi}{\partial\eta^2} + Pe\frac{\partial\phi}{\partial\eta} - 2B\phi - 0 \tag{9}$$

For a long rod, the boundary conditions are:

at $\eta = 0$:

$$\phi - 1 \tag{10}$$

and at $\eta \to \infty$:

$$\phi - 0 \tag{11}$$

The solution of equation 9 is:

$$\phi - \exp[-(\frac{Pe + \sqrt{Pe^2 + 8B}}{2})\eta] \tag{12}$$

or

$$T(z) - T_h + (T_h - T_0)\exp(-\Psi z) \tag{13}$$

where T_O is the temperature of the interface and Ψ is given by:

$$\Psi - \frac{Pe + \sqrt{Pe^2 + 8B}}{2R} \tag{14}$$

From this the temperature gradient in the melt is:

$$\frac{\partial T}{\partial z} - \zeta\exp[-\Psi z] \tag{15}$$

5

where

$$\zeta - \Psi(T_h - T_E)$$ (16)

Substituting equation 15 into equation 7, we obtain:

$$\nabla^2 C + \frac{V}{D}\frac{\partial C}{\partial z} - \frac{D'}{D}\zeta\frac{\partial[C\exp(-\Psi z)]}{\partial z} - 0$$ (17)

To solve equation 17, we use the same boundary conditions at the interface as described by Jackson and Hunt [3]. On the other hand, the appropriate boundary condition far from the interface is not clear. Because the temperature gradient extends far into the melt, the concentration variation also extends far into the melt. Since a numerical solution appears to be necessary, a large domain would present serious computational difficulties. To avoid this problem we recognize that the concentration variation becomes essentially one dimensional at some small distance from the interface. Thus we break our problem into two parts. Far from the interface the variation in concentration is one dimensional and can be found analytically. Near the interface the variation in concentration is three-dimensional and must be found numerically. Where these two domains meet, the concentration and its gradient must be the same for both solutions.

The concentration in the liquid far from the solid/liquid interface is found by solving equation 17 written for one dimensional transport:

$$\frac{\partial^2 \overline{C}}{\partial z^2} + \frac{V}{D}\frac{\partial \overline{C}}{\partial z} - \frac{D'}{D}\zeta\frac{\partial[\overline{C}\exp(-\Psi z)]}{\partial z} - 0$$ (18)

where $\overline{C}$ is the average concentration at position z. The boundary conditions necessary to solve equation 18 during the growth of an eutectic are, as shown in figure 1:

at $z \to \infty$:

$$\overline{C}(z\to\infty) - C_E$$ (19)

6

At $z=0$ the average melt concentration is assumed to be the eutectic:

$$\overline{C}(z=0) = C_E \tag{20}$$

We find by integrating equation 18 twice:

$$\overline{C}(z) = \frac{C_E \dfrac{V}{D} \displaystyle\int_0^z \exp\left[\dfrac{V}{D}z + \dfrac{D'\zeta}{D\Psi}\exp(-\Psi z)\right]dz + C_E \exp\left(\dfrac{D'\zeta}{D\Psi}\right)}{\exp\left[\dfrac{V}{D}z + \dfrac{D'\zeta}{D\Psi}\exp(-\Psi z)\right]} \tag{21}$$

For the three-dimensional numerical solution the boundary condition at the solid/liquid interface ($z=0$) is found by a material balance which takes into account the Soret effect, normal diffusion and flow of melt into the solid (see figure 2).
Then over the α phase:

$$\left(\frac{\partial C}{\partial z}\right)_{z=0} = -\frac{V}{D}(C_i - C_S^\alpha) + C_i\frac{D'}{D}\zeta \tag{22}$$

and over the β phase:

$$\left(\frac{\partial C}{\partial z}\right)_{z=0} = -\frac{V}{D}(C_i - C_S^\beta) + C_i\frac{D'}{D}\zeta \tag{23}$$

A regular eutectic rod structure repeats itself periodically in both x and y directions. Therefore the computational domain will be a rectangular area as presented in figure 3. (The interface presents a similar structure to the one described in [3]). The fibers (β phase) are located on the corners of a hexagon. Under such a case, the periodic boundary conditions are:

$$C_{x=0} = C_{x=\lambda} \tag{24}$$

and

$$C_{y=0} = C_{y=\sqrt{3}\lambda} \tag{25}$$

7

To reduce the number of variables, equation 7 was also non-dimensionalized. The scaling variables are $X=x/\lambda$, $Y=y/\lambda$ and $Z=z/\lambda$. The non-dimensional equation is:

$$\nabla^2 W + \Lambda\frac{\partial W}{\partial Z} - \Gamma\Theta\frac{\partial[W\exp(-\Theta Z)]}{\partial Z} = 0 \qquad (26)$$

where $W=C/C_E$, $\Lambda=\lambda V/D$ is a rod spacing based Peclet number, $\Gamma=(T_h-T_E)D'/D$ is a Soret parameter and $\Theta=\lambda\Psi$ is a function of Biot and Peclet numbers. For example, for $\lambda=0.001m$ and typical experimental conditions, $\Lambda=0.1$, $\Gamma=20$ and $\Theta=0.003$. These values were obtained from conditions generally found during crystal growth, i.e. Biot number close to 0.25 and Peclet number close to $2.5x10^{-4}$. Based on our prior experience [9,11], we note that lateral disturbances to the concentration are almost completely damped out by $z=3\lambda$. At this position the 3d numerical solution must match the 1d analytical solution, equation 21. Thus from the non-dimensionalized form of equation 21, we obtain the boundary condition at $Z=3$:

$$\overline{W}(3) = \frac{\Lambda\int_0^3\exp[\Lambda Z + \Gamma\exp(-\Theta Z)]dZ + \exp(\Gamma)}{\exp[\Lambda Z + \Gamma\exp(-\Theta Z)]} \qquad (27)$$

At $Z=0$, equation 22 becomes:

$$\left(\frac{\partial W}{\partial Z}\right)_{Z=0} = -\Lambda(W_i - W_S^\alpha) + W_i\Gamma\Theta \qquad (28)$$

and over the β phase, from equation 23:

$$\left(\frac{\partial W}{\partial Z}\right)_{Z=0} = -\Lambda(W_i - W_S^\beta) + W_i\Gamma\Theta \qquad (29)$$

The periodicity condition in the x and y directions yields the following boundary conditions:

$$W_{X=0} = W_{X=1} \qquad (30)$$

and

$$W_{Y-0} - W_{Y-\sqrt{3}}$$ (31)

The solution of this set of equations was found by writing equation 26 in an explicit finite difference form, which was solved by using the Successive Over Relaxation Technique. To simulate a rod eutectic structure, the fibers and the matrix were approximated by an array of square elements as described elsewhere [11].

3. RESULTS AND DISCUSSION

Figure 4 presents profiles of average liquid concentration as a function of distance, for several values of Γ, $\Lambda=0.1$ and $\Theta=0.003$. The 3d model was applied to calculate the liquid concentration profile for a eutectic concentration $C_E=0.03$. To reduce computational complexities, the mutual solid solubilities of the α and β phases were assumed to be negligible, so that the composition of these phases were equal to 0 and 1, respectively. A three-dimensional plot of the liquid composition at the rod-like eutectic interface is shown in figure 5. In this figure, the difference between the composition over the fibers and the matrix is clear. The concentration of B over the β phase is much lower than over the α phase, which results from the demand of B atoms to form the fibers and vice-versa.

According to Jackson and Hunt [3], the total undercooling ΔT at a solid/liquid eutectic interface is the sum of that arising from the deviation of the liquid composition from the eutectic and that due to the curvature of the interface. Thermal diffusion is expected to change the interfacial liquid composition, and thereby change the rod spacing. Using an approach similar that used to examine the influence of convection [7], the undercooling ΔT at any interfacial position is:

$$\Delta T - K_1(\overline{W_i} - W_E) + \frac{K_2}{\lambda}$$ (32)

9

where $\overline{W} - \overline{C}/C_E$.

The term for the composition change can be represented by two parts:

$$(\overline{W}_i - W_E) - (\overline{W}_i - W_E)_{JH} - \Delta \tag{33}$$

where Δ is the change due to the Soret effect. The subscript JH means the composition difference found by Jackson and Hunt in the absence of Soret effect:

$$(\overline{W}_i - W_E)_{JH} - A\Lambda \tag{34}$$

By calculating the average undercooling for each phase and assuming constant total undercooling, $\Delta T = \Delta T_\alpha = \Delta T_\beta$, the constants K_1 and K_2 were found to be:

$$K_1 - \frac{m_\alpha m_\beta}{m_\alpha + m_\beta} \tag{35}$$

and

$$K_2 - \frac{4K_1}{\sqrt{1 - C_E}} \left[\frac{K_\alpha}{m_\alpha} + \frac{K_\beta(1 - C_E)}{m_\beta C_E} \right] \tag{36}$$

where m is the slope of the liquidus line, K_α and K_β are constants relating λ to the undercooling changes due to curvature, as defined in [3]. The value of A is:

$$A - A_\alpha + A_\beta \tag{37}$$

where

$$A_\alpha - 2M \tag{38}$$

and

$$A_\beta - \frac{2(1 - C_E)M}{C_E} \tag{39}$$

10

M is obtained by [3]:

$$M - \sum_{n-1}^{-} \frac{1}{(n\pi)^3} \left[\frac{J_1\left(n\pi\sqrt{1-C_E}\right)}{J_0(n\pi)} \right]^2 \tag{40}$$

Finally, Δ is written as:

$$\Delta - \Delta_\alpha + \Delta_\beta \tag{41}$$

where the composition difference from the eutectic for each solid phase is given by:

$$\Delta_\alpha - (\overline{W_i^\alpha} - W_E)_{JH} - (\overline{W_i^\alpha} - W_E) \tag{42}$$

and

$$\Delta_\beta - (W_E - \overline{W_i^\beta})_{JH} - (W_E - \overline{W_i^\beta}) \tag{43}$$

By differentiating equation 32 with respect to the rod spacing λ and setting the result equal to zero, the extremum condition is found to be given by [3]:

$$\lambda^2 - \frac{K_2 D}{K_1 A V \left(1 - \frac{D}{AV} \frac{\partial \Delta}{\partial \lambda}\right)} \tag{44}$$

Without thermal diffusion, $\Delta = 0$ and the rod spacing is given by:

$$\lambda_0^2 - \frac{K_2 D}{K_1 A V} \tag{45}$$

Substituting equation 45 into equation 44 results in:

$$\left(\frac{\lambda}{\lambda_0}\right)^2 - \left(1 - \frac{D}{AV} \frac{\partial \Delta}{\partial \lambda}\right)^{-1} \tag{46}$$

11

The analysis of the numerical results showed that for constant C_E, Γ and Θ, Δ is virtually independent of Λ. Figure 6 presents Δ as a function of Λ for several intensities of thermodiffusion. Examination of the curves in this figure allows one to write:

$$\Delta - \Lambda f(\Gamma) \qquad (47)$$

The term $\partial \Delta / \partial \lambda$ in 46 is given by:

$$\frac{\partial \Delta}{\partial \lambda} - \frac{\partial \Lambda}{\partial \lambda} f(\Gamma) + \Lambda \frac{\partial f(\Gamma)}{\partial \Gamma} \frac{\partial \Gamma}{\partial \lambda} \qquad (48)$$

Since Γ is independent of λ, the substitution of equation 48 into equation 46, yields:

$$\left(\frac{\lambda}{\lambda_o}\right)^2 - \left[1 - \frac{f(\Gamma)}{A}\right]^{-1} \qquad (49)$$

Figure 7 shows numerical results of $f(\Gamma)$ as a function of Γ, for $\Lambda = 0.1$ and Θ equal to 0.003 and 0.03. The thermal diffusion phenomenon decreases the changes of the interfacial liquid composition linearly with increase of the thermal diffusion coefficient. The examination of both cases ($\Theta = 0.003$ and 0.03), showed that the variation in the melt composition is essentially the same for those values of Θ. Then, apparently the deviation in interfacial composition is only slightly dependent of Θ. This result leads to the hypothesis that changes in the Biot and Peclet numbers, within the range studied, have only small influences on the effect of thermal diffusion on the eutectic microstructure. Figure 8 presents λ/λ_0 as a function of Γ, for $\Theta = 0.003$ and $\Theta = 0.03$. By increasing the thermal diffusion effect (Γ), the microstructure is expected to become finer. On the other hand, if the sign of the thermal diffusion coefficient is changed (the solute migrates to the coldest end), the microstructure should coarsen. A polynomial fit for λ/λ_0 as a function (Γ) produces:

$$\frac{\lambda}{\lambda_0} - 1 - 1.2 x 10^{-4} \Gamma + 2.0 x 10^{-8} \Gamma^2 \qquad (50)$$

The influence of the Soret effect on the rod-like structure, using typical experimental values ($\Gamma = 10$ $\theta = 0.003$ and $\Lambda = 0.1$), shows a variation very small ($\lambda/\lambda_0 \approx 1$) compared to the same process without this effect. The change obtained is not sufficient to explain the finer structure obtained in samples processed in space.

4. CONCLUSIONS

The results obtained during this theoretical analysis show that the presence of thermal diffusion during rod eutectic solidification may change the fiber spacings. This change is due to a change in the liquid composition at the interface. The average interfacial composition varies linearly with the thermal diffusion coefficient. Also, the results show that the influence of thermal diffusion on the eutectic solidification is little affected by the Biot and Peclet numbers within the ranges studied here. With reasonable values of the parameters, we found that the Soret effect is not enough to explain the change obtained in space.

ACKNOWLEDGEMENT

NOMENCLATURE
Parameters

A Jackson-Hunt constant for fiber spacing

B hR/k, Biot number

C Mass fraction of component B (wt%)

C_P Heat capacity (J m^{-3} K^{-1})

D Diffusion coefficient in the melt (m^2 s^{-1})

D' Thermal diffusion coefficient (m^2 s^{-1} K^{-1})

$f(\Gamma)$ $\Delta(\Gamma)/\Lambda$

h Heat transfer coefficient (W m^{-2} K^{-1})

13

K	Constant defined in equation 35 and 36
k	Thermal conductivity (W m^{-1} K^{-1})
M	Function defined by Jackson and Hunt for the analytical solution of equation 26 [3]
m	Slope of the liquidus line (K wt%$^{-1}$)
Pe	$\rho C_P VR/k$, Peclet number
R	Radius of the sample (m)
T	Temperature in the melt (K)
V	Freezing rate (m s^{-1}).
x,y	Distances along the solid/liquid interface (m)
X,Y	Dimensionless distances along the solid/liquid interface, x/λ and y/λ
z	Distance into the melt from the interface (m)
Z	Dimensionless distance into the melt from the interface, z/λ
W	C/C_E, Dimensionless concentration
Δ	$(\overline{W_i^\alpha - W_E})_{JH} - (\overline{W_i^\alpha - W_E})$ for α phase and $(W_E - \overline{W_i^\beta})_{JH} - (W_E - \overline{W_i^\beta})$ for β phase
μ	Viscosity of the melt (m^2 s^{-1})
ρ	Density of the melt (Kg m^{-3})
λ	Spacing between the rods (m)
Γ	$(T_h\text{-}T_E)D'/D$, Soret parameter
Θ	$\lambda\Psi$, Thermal decay distance
Λ	$\lambda V/D$, Freezing rate based Peclet number

Subscripts and Superscripts

E	Eutectic
h	Heater
i	Interfacial
JH	Pure diffusion growth process, as done by Jackson and Hunt.
α	Alpha phase
β	Beta phase

REFERENCES

[1]   C. Zener, AIME Trans. 167 (1946) 550.

[2]   W. H. Brandt, J. Appl. Phys. 16 (1945) 139.

[3]   K. A. Jackson and J.D. Hunt, Trans. AIME 236 (1966) 1129.

[4]   R. G. Pirich and D.J. Larson, in: Materials Processing in Reduced Gravity Environment of Space, Ed. G.E. Rindone (North - Holland, New York, 1982) p. 253.

[5]   R. G. Pirich, G. Bush, W. Poit and D.J. Larson, Jr, Met. Trans. 11A (1980) 193.

[6]   G. Muller and P. Kyr, in: Proc. 15th European Symp. on Materials Science under Microgravity, Schloss Elmau, Nov. 1984, ESA SP-222, p.141.

[7]   V. Baskaran and W.R. Wilcox, J. Crystal Growth 67 (1984) 343.

[8]   S. Chandrasekhar, PhD Thesis, Clarkson University, Potsdam (1987).

[9]   S. Chandrasekhar, G.F. Eisa and W.R. Wilcox, J. Crystal Growth 78 (1986) 485.

[10] G. F. Eisa and W.R. Wilcox, J. Crystal Growth 78 (1986) 159.

[11] R. Caram, S. Chandrasekhar and W.R.Wilcox, to be published, J. Crystal Growth.

[12] S. R. de Groot, Physica IX 7 (1942) 699.

[13] D. R. Caldwell, J. Phys. Chem. 79 (1975) 17.

[14] A. S. Yue, J. Crystal Growth 42 (1977) 542.

[15] A. S. Yue, J. Phys. Chem. Solids Suppl. 328 (1967) 197.

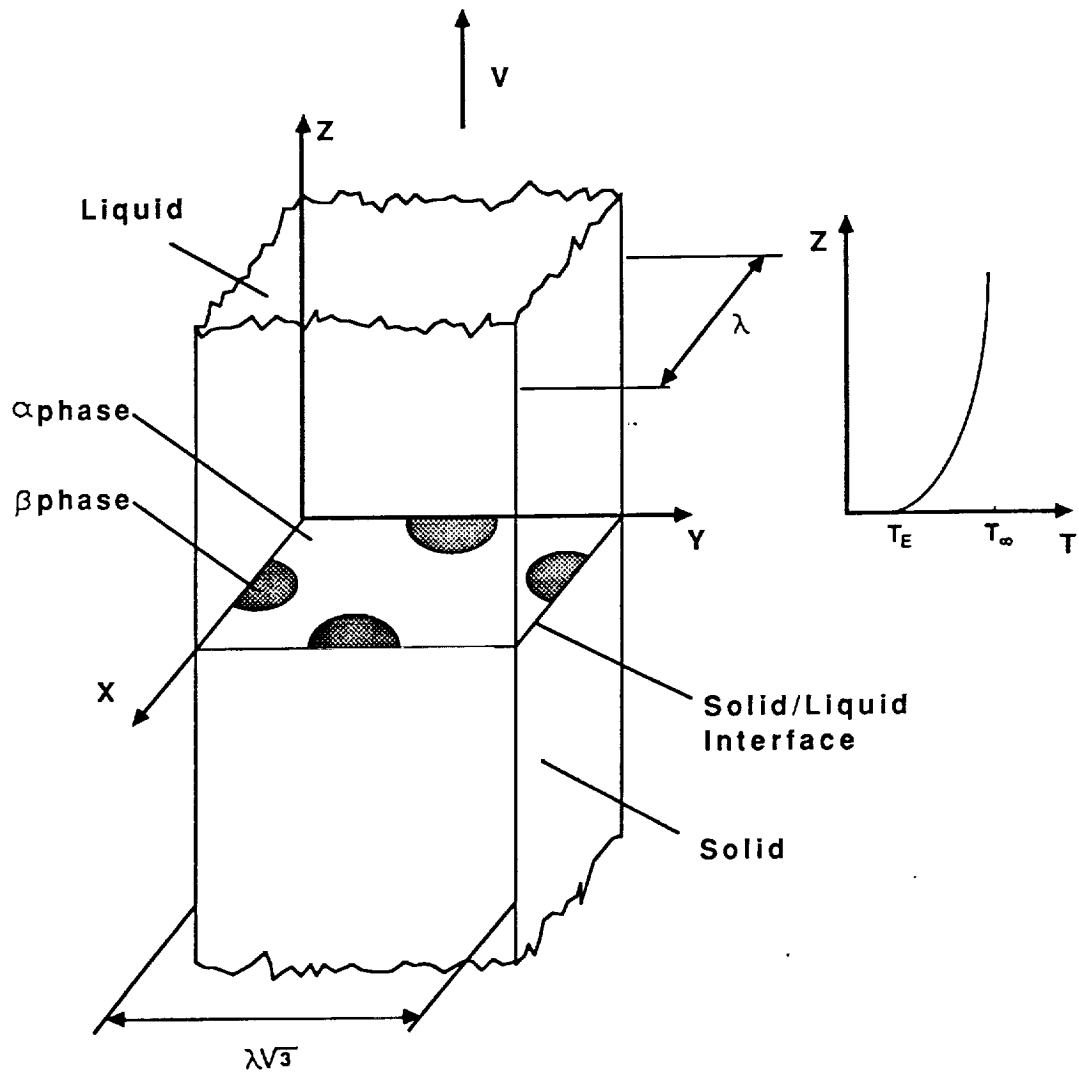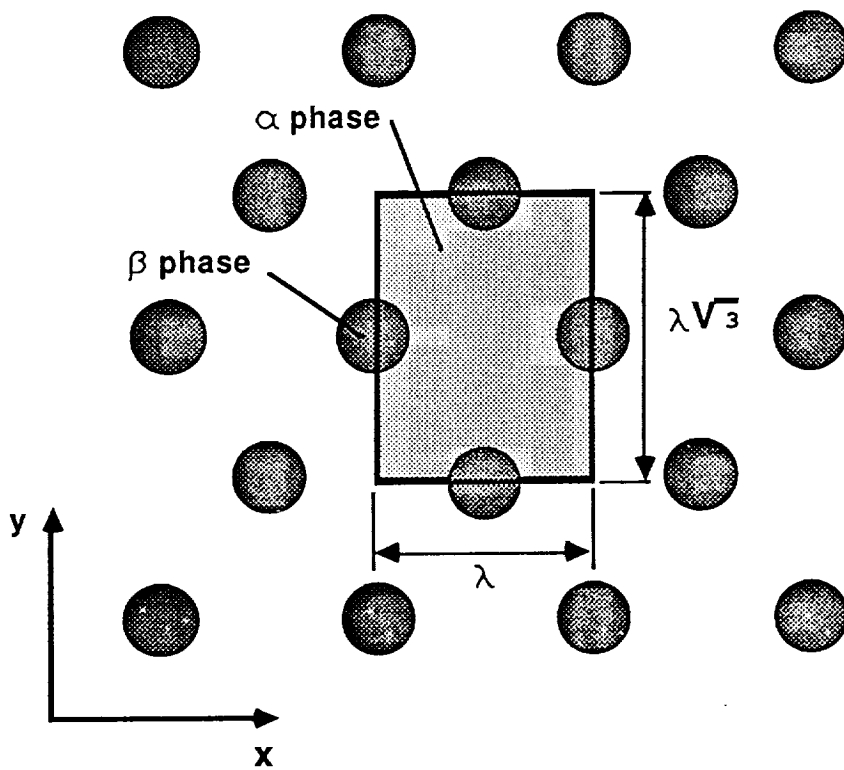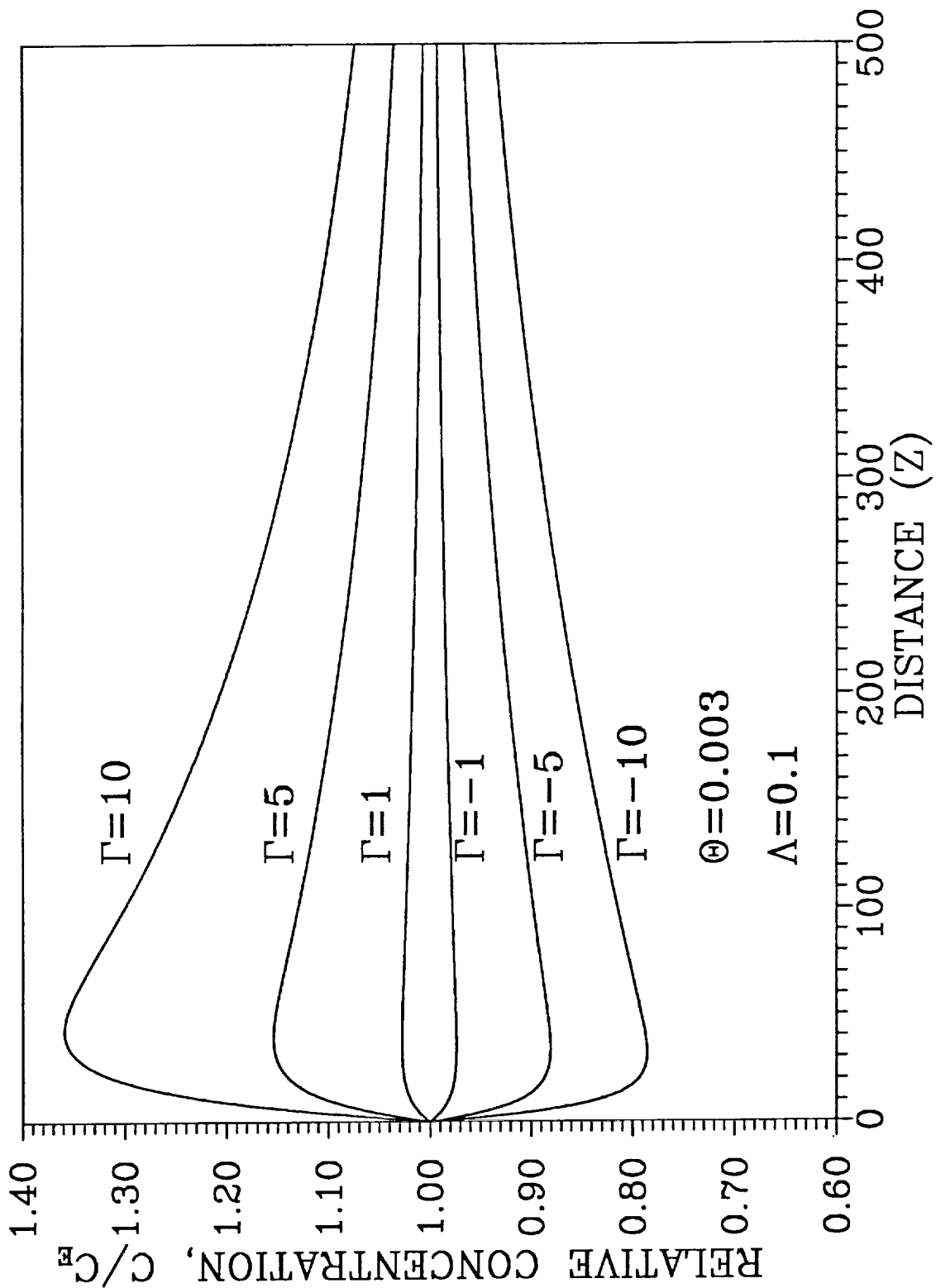[16] A. S. Yue and J. T. Yue, J. Crystal Growth 13/14 (1972) 797.
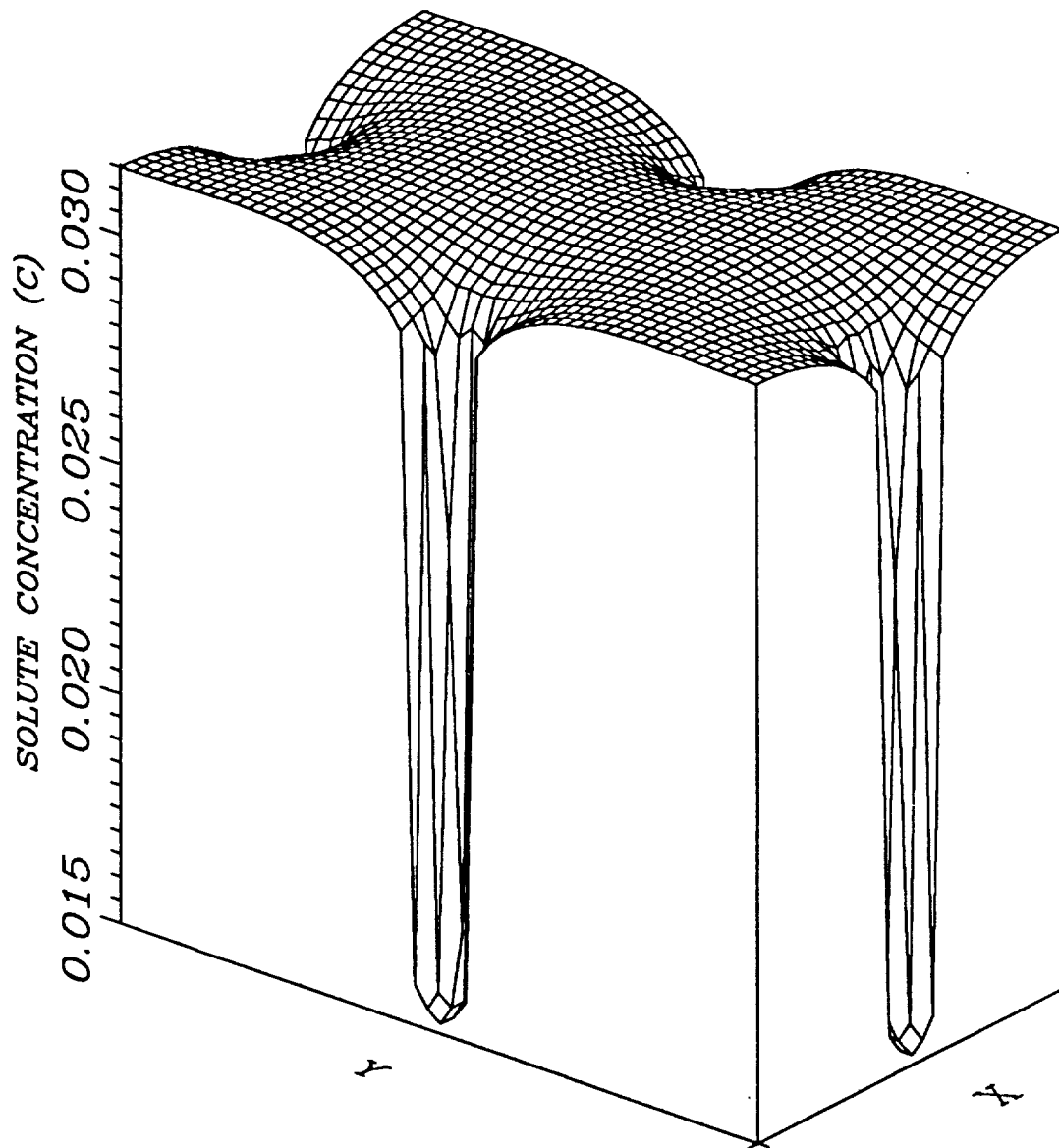
LIST OF FIGURES

FIGURE 1

FIGURE 2

FIGURE 3
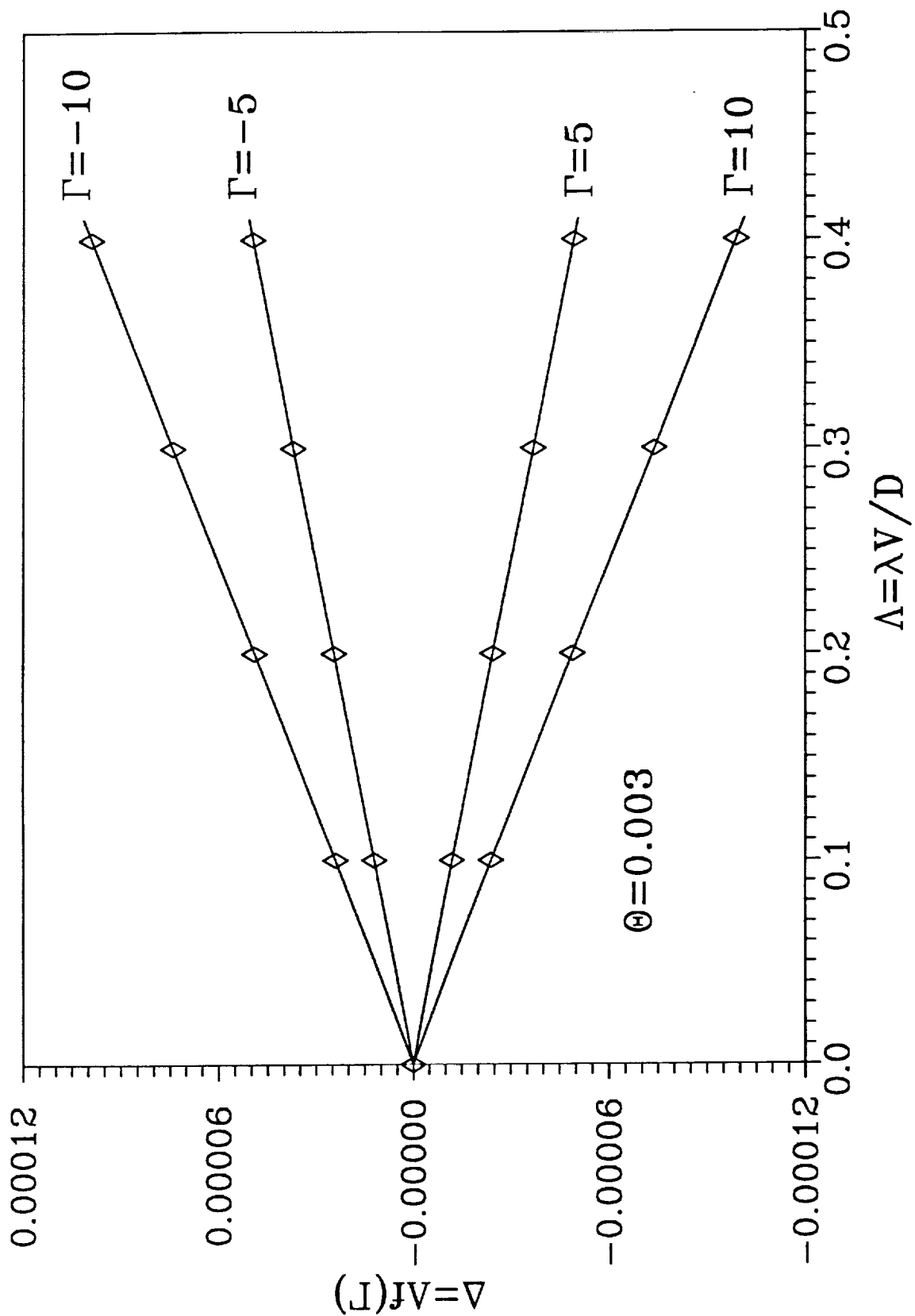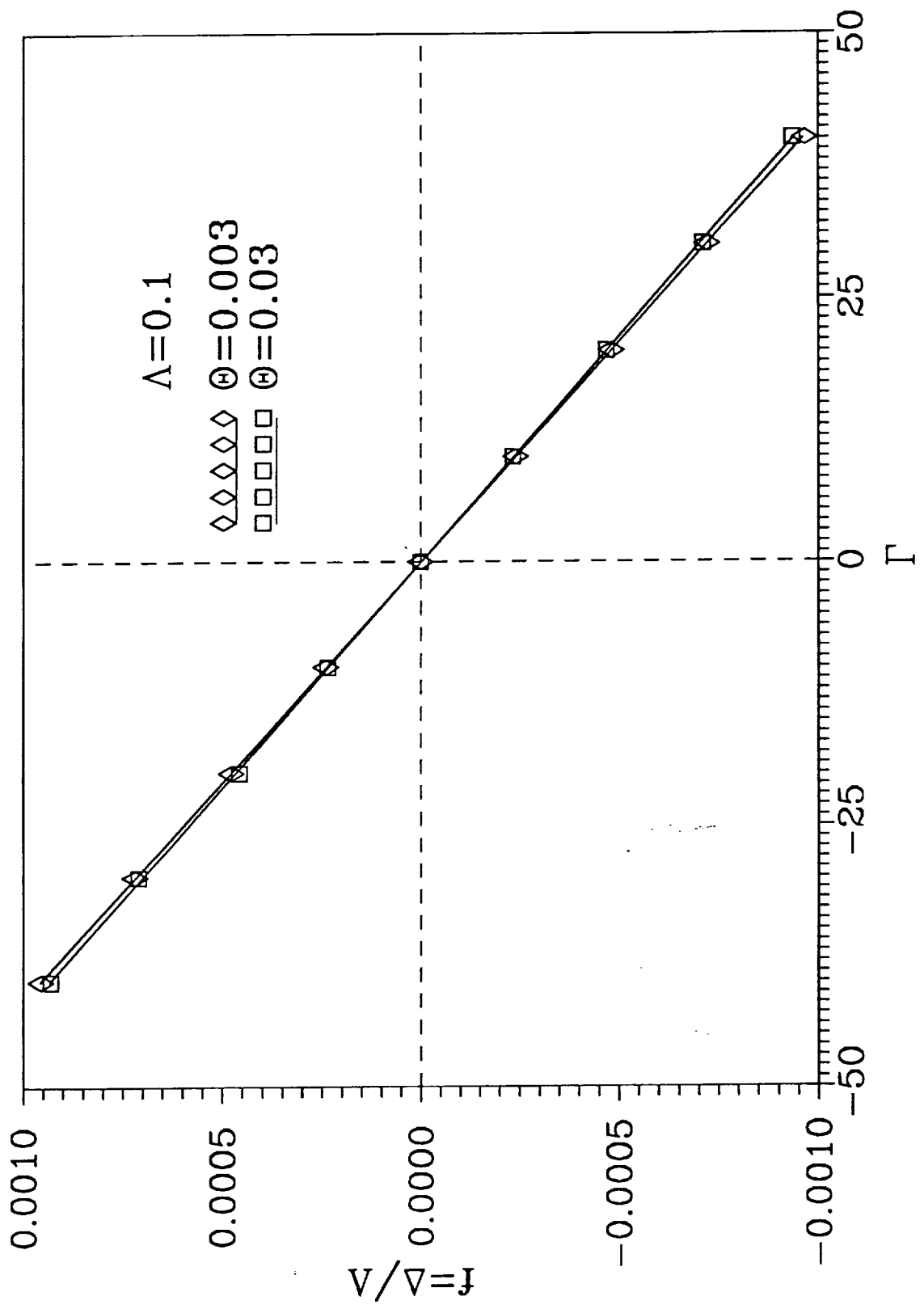
FIGURE 4

FIGURE 5

FIGURE 6
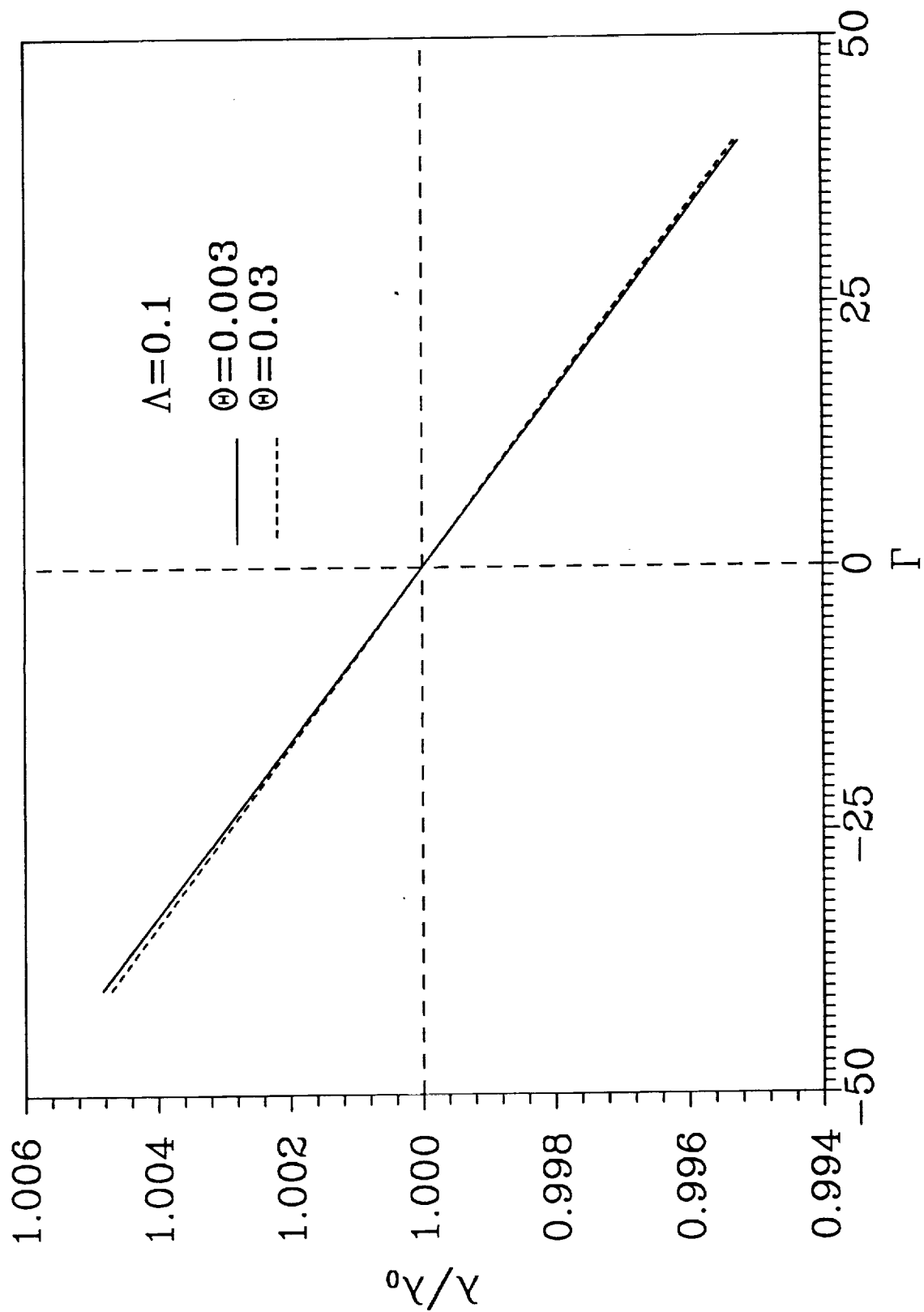
FIGURE 7

FIGURE 8

APPENDIX   B

EXCERPTS FROM A.P. MOHANTY'S M.S. THESIS

"DETERMINATION OF THE SORET COEFFICIENT OF Mn-Bi MELTS"

Chapter 3

Experiments

This chapter gives the details of the equipment, the experiment and the analysis of the samples. As mentioned in the chapter before, it was desired to obtain a convection free environment. Also, as shown in the next chapter, a linear temperature profile was desired. A detailed description of the apparatus and the experimental procedure is given in the following pages.

3.1 Apparatus

An important part of the project was the design of the apparatus. Many different options were considered. A schematic of the final apparatus is shown in figure 3.1. The apparatus can be divided into three main sections:

- The furnace

- The ampoule

- The temperature control unit

3.1.1 Furnace

The core of the furnace consisted of a metal rod with a 5mm hole drilled through it. The diameter of the rod was 0.5 inch (1.27 cm). The rod was to be thick enough so that there was a good chance of obtaining a linear temperature profile. The limiting
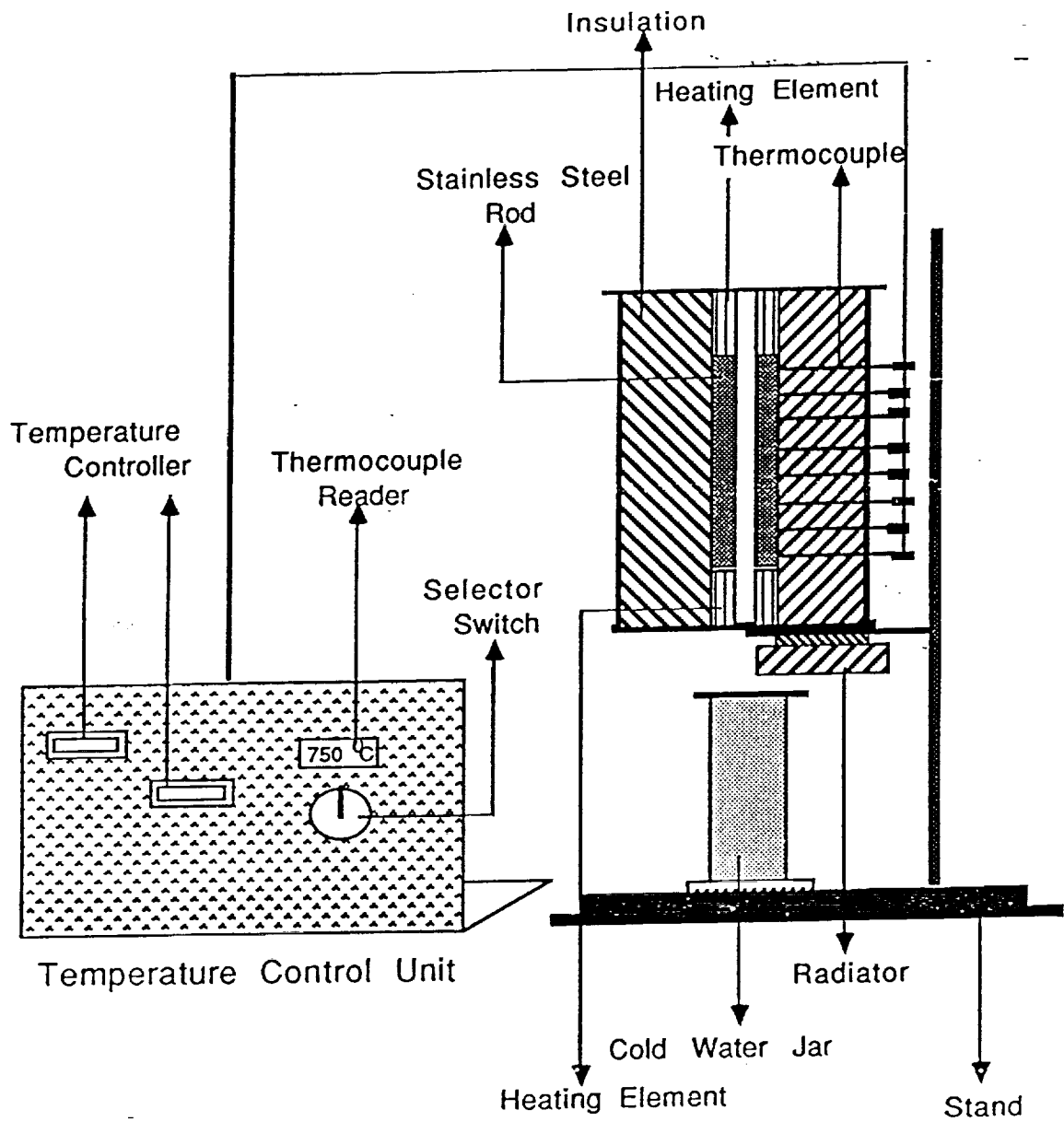
Figure 3.1: Schematic diagram of the apparatus used for the experiments.

factor on the diameter of the rod was the machinability of the metal. Initially a brass rod was used, but after a few runs the brass oxidized and there was some reaction between the quartz and the brass. In figure 3.2 there are some pictures showing the oxidized brass. To avoid oxidation, a stainless steel rod (AISI type 446) was used and worked well. The gap between the ampoule wall and the inner wall of the furnace had to be as small as possible, so as to reduce air drafts. The ampoule was expected to be 3mm in outer diameter. Thus the furnace being 5mm ID gave some room for changes in ampoule diameter and for the furnace not to be perfectly straight.

The furnace was positioned vertically and had two heaters at the ends. The two ends of the steel rod were machined down so that a quartz tube could slide over the ends. Figure 3.3 shows the heater. The heater consisted of Kanthal wire wound on the quartz tube. The top heater was maintained at a higher temperature than the bottom heater. To ensure that the turns of the heater resistance wire did not touch each other, the heater element was protected with porcelain fish spine (Omega Engineering, Inc.).

Furnace characteristics:

Hot zone:

- Input voltage: 8 volts

- Temperature:700°C

- Heater electrical resistance: 5Ω

Cold zone:

- Input voltage:4 volts

- Temperature: 400°C

- Heater electrical resistance: 5Ω

The whole furnace was mounted on a stand. The bottom end of the furnace was kept closed with a flat piece of metal. The metal piece at the bottom of the furnace was not fixed and could be easily removed. Below the furnace was a cylindrical jar with ice water. At the end of an experiment the metal piece was pulled out and the ampoule containing the material was slipped down into the jar of ice water and thereby quenched. The whole furnace was well insulated with three layers of an alumina based ceramic fiber insulation (Cotronics corporation). Each layer of insulation was about 0.5 cm thick. Some pictures of the furnace are shown in the following pages.

3.1.2 Ampoule

The ampoule was designed to limit the convection in the melt. As mentioned before, convection is governed by the Grashof number. One way of keeping the Grashof number, and hence the convection, low is to have a small diameter. After loading the material the ampoule was sealed under vacuum. The cleaning and loading procedure is described later in this chapter. The small diameter of the ampoule made it difficult to work with. It was difficult to get any fluid into the thinner section of the ampoule, which made it difficult to clean. The material had to be ground to a fine powder to be able to load the ampoule. An ampoule of a smaller diameter would have made it even more difficult to clean and load. Considering the above factors, an inner ampoule diameter of 1mm was reasonable.

The outer diameter of the top end of the ampoule had to be 11 mm because it was the smallest diameter that the vacuum system in the laboratory could handle. The bottom end of the ampoule had to be open because it was not possible to force any kind of liquid into the thinner part of the ampoule with one end closed. A quartz ampoule is shown in figure 3.4. Quartz was preferred over other materials because of the extended period of the experiment and the temperature range.
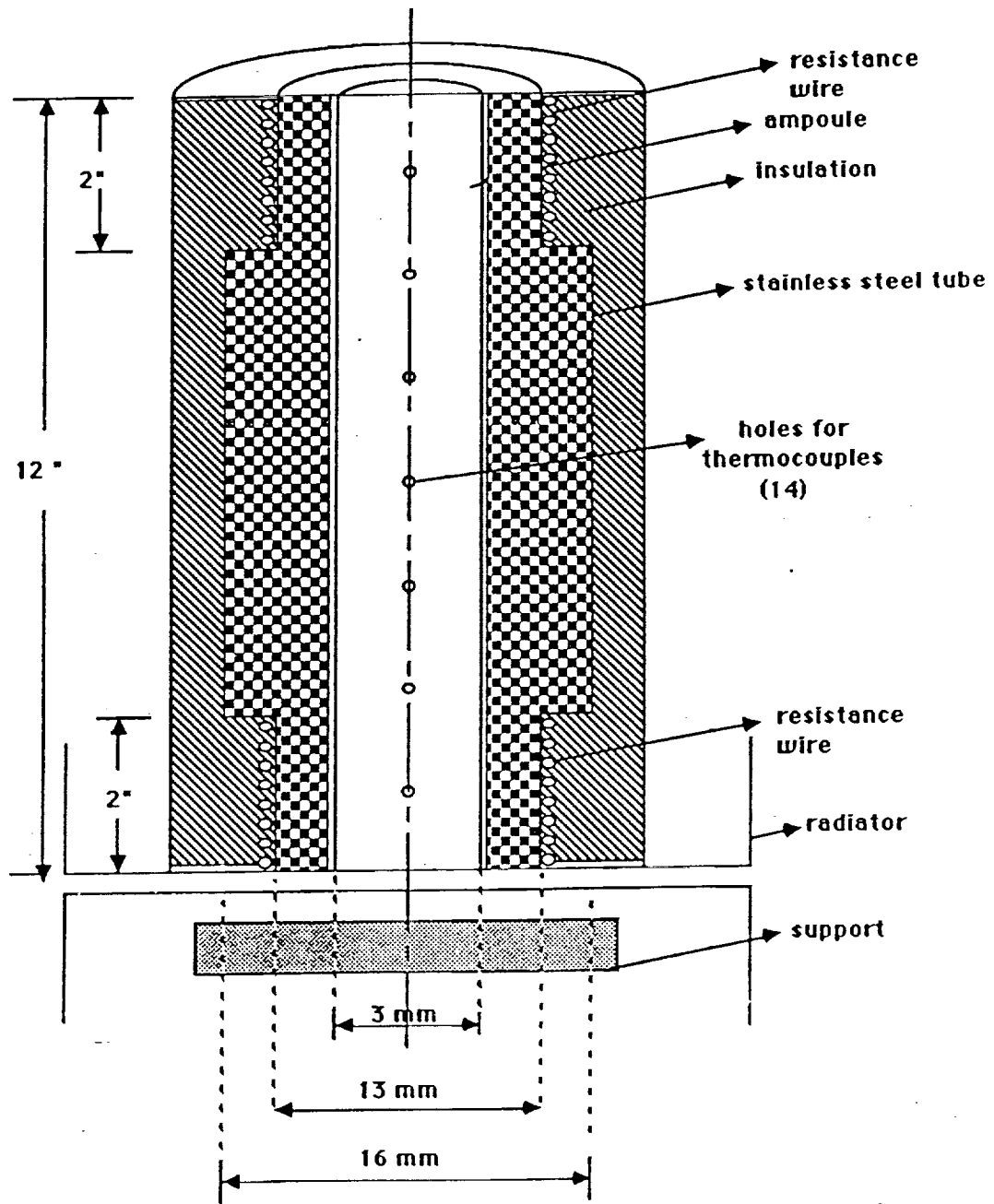
23

Figure 3.3: Longitudinal cross-section of the furnace showing the two heaters and the holes for the thermocouples along the length of the furnace.

The upper limit of temperature in the experiment was 800° C and fused quartz softens at about 1400° C.

3.1.3 Temperature Control Unit

The temperature was measured along the length of the furnace with type K thermocouples. Small holes were drilled at regular intervals of 1.6 mm and the thermocouples were introduced through these such that they touched the ampoule wall. To read the temperature, the thermocouples were connected to a digital thermocouple reader (Omega Engineering, Inc.) through a selector switch. The thermocouples in the heaters were connected to the temperature controllers (Eurotherm Corporation).

The temperatures in the two heaters were controlled by two separate controllers. The current and voltage could be varied with the two Variacs in the control unit. The temperature was displayed by the digital thermometer on the panel. All the thermocouples were connected to the display through a selector switch. There was also a fuse box and a number of electrical output sockets on the control unit. The whole unit was mounted on wood.

Although the temperature profile along the wall of the ampoule could be approximated by a linear fit, a second degree polynomial fit the data more closely. Some typical profiles are shown in figure 3.5 and figure 3.6. The polynomial fit is shown in figure 3.7 and figure 3.8. The temperature profile obtained with the stainless steel core was used in all the experiments.

11mm   OD

10 cm

30 cm
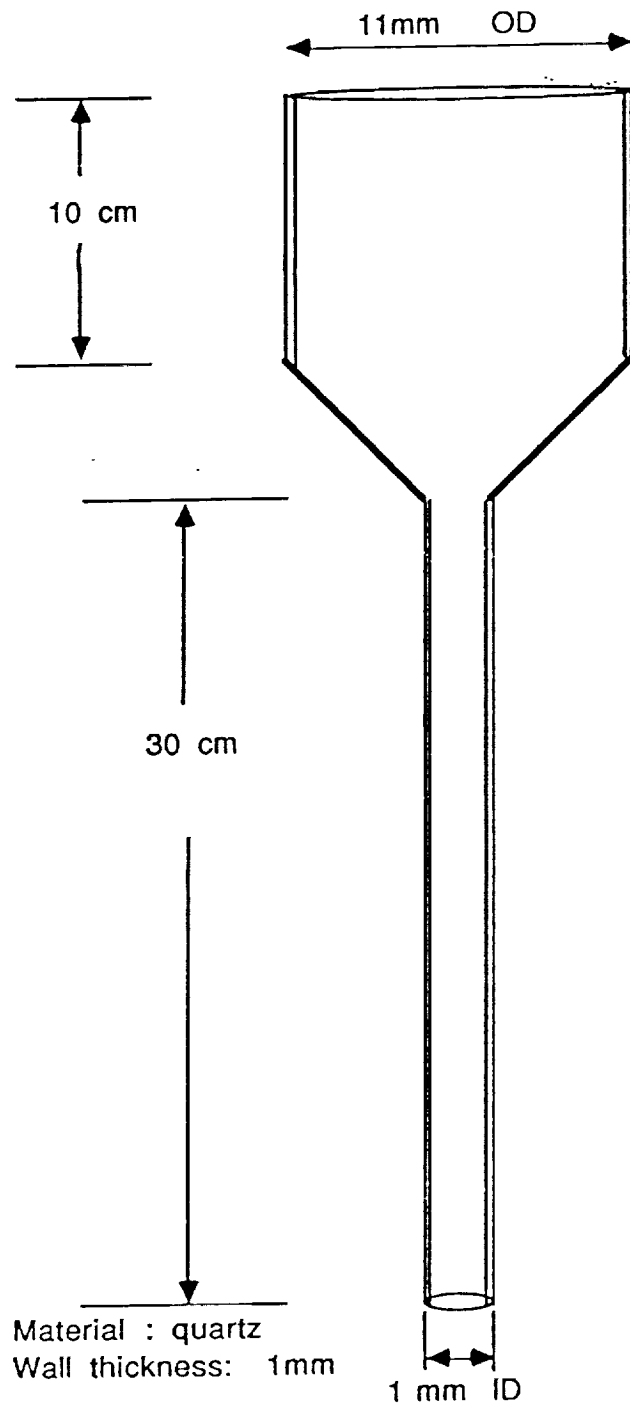
Material : quartz
Wall thickness: 1mm

1 mm ID

Figure 3.4: Design of the ampoule used to load the material in the furnace. The broad part of the ampoule was cut off after sealing the ampoule.
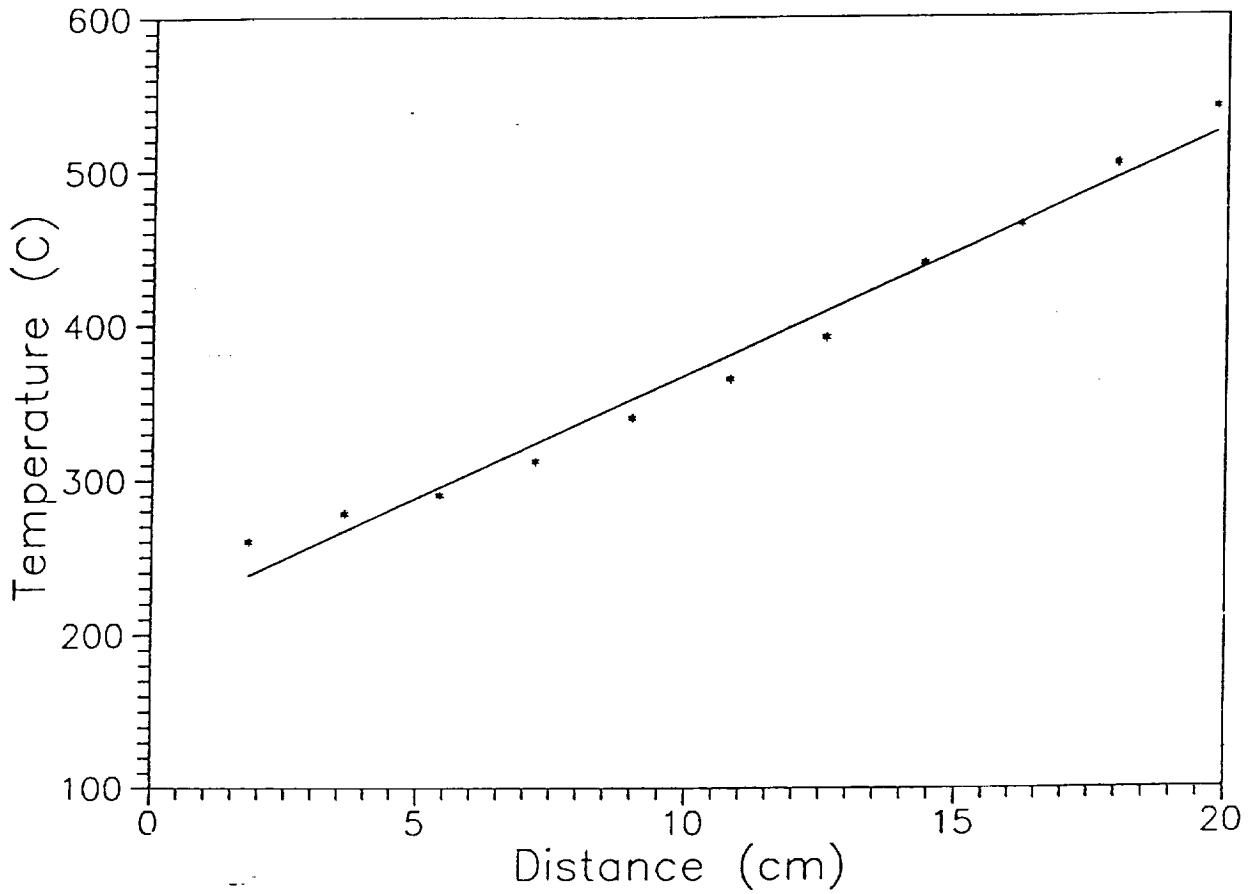
Figure 3.5: Experimentally determined temperature profile along the wall of the ampoule with a brass core. The line is a least squares fit to the data. The equation of the line is $T = 15x + 209$ where T is temperature in °C and x is distance in cm.
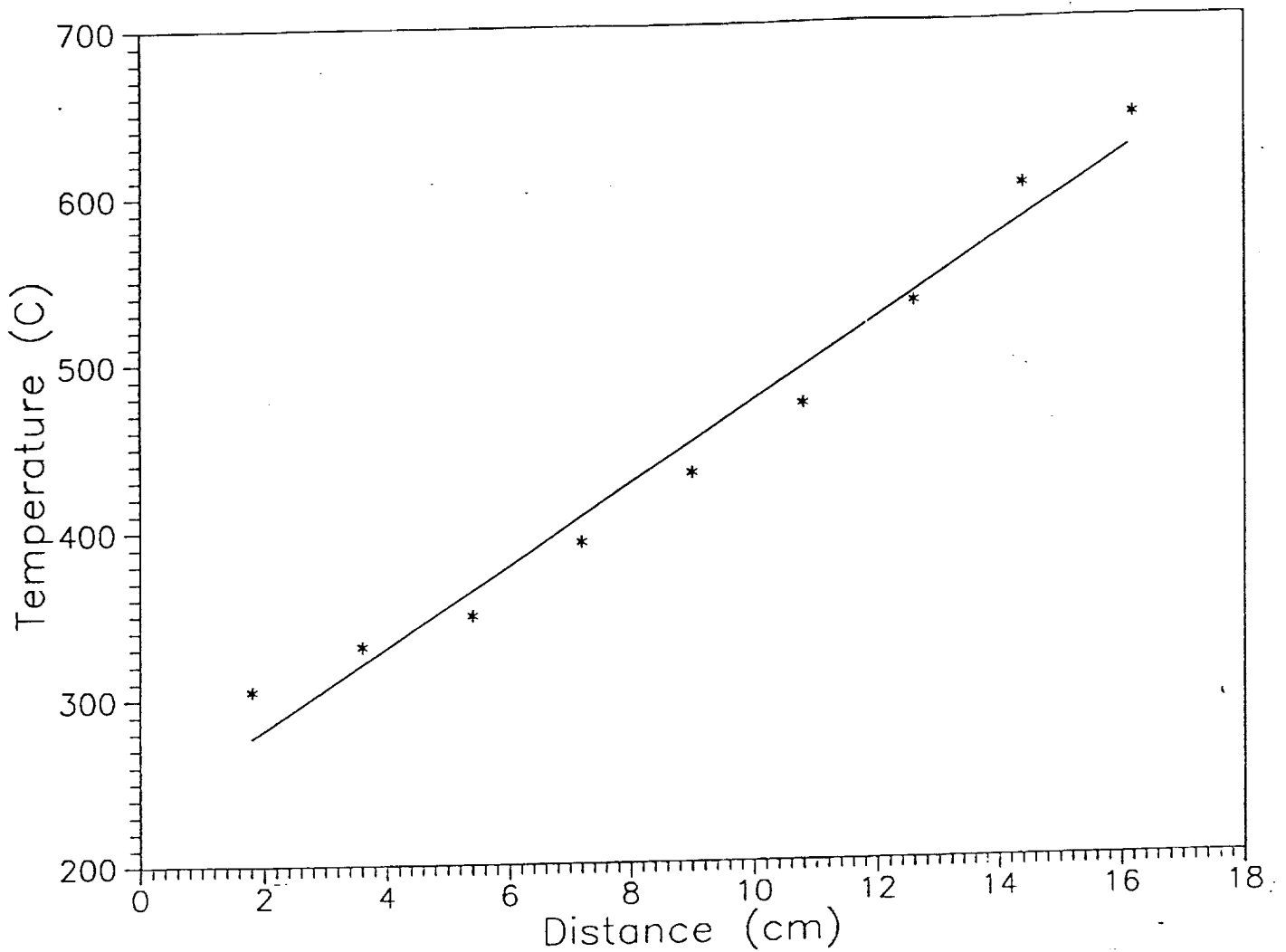
Figure 3.6: Experimentally determined temperature profile along the wall of the ampoule with a stainless steel core. The line is a least squares fit to the data. The equation of the line is T = 24x + 233 where T is temperature in °C and x is distance in cm.
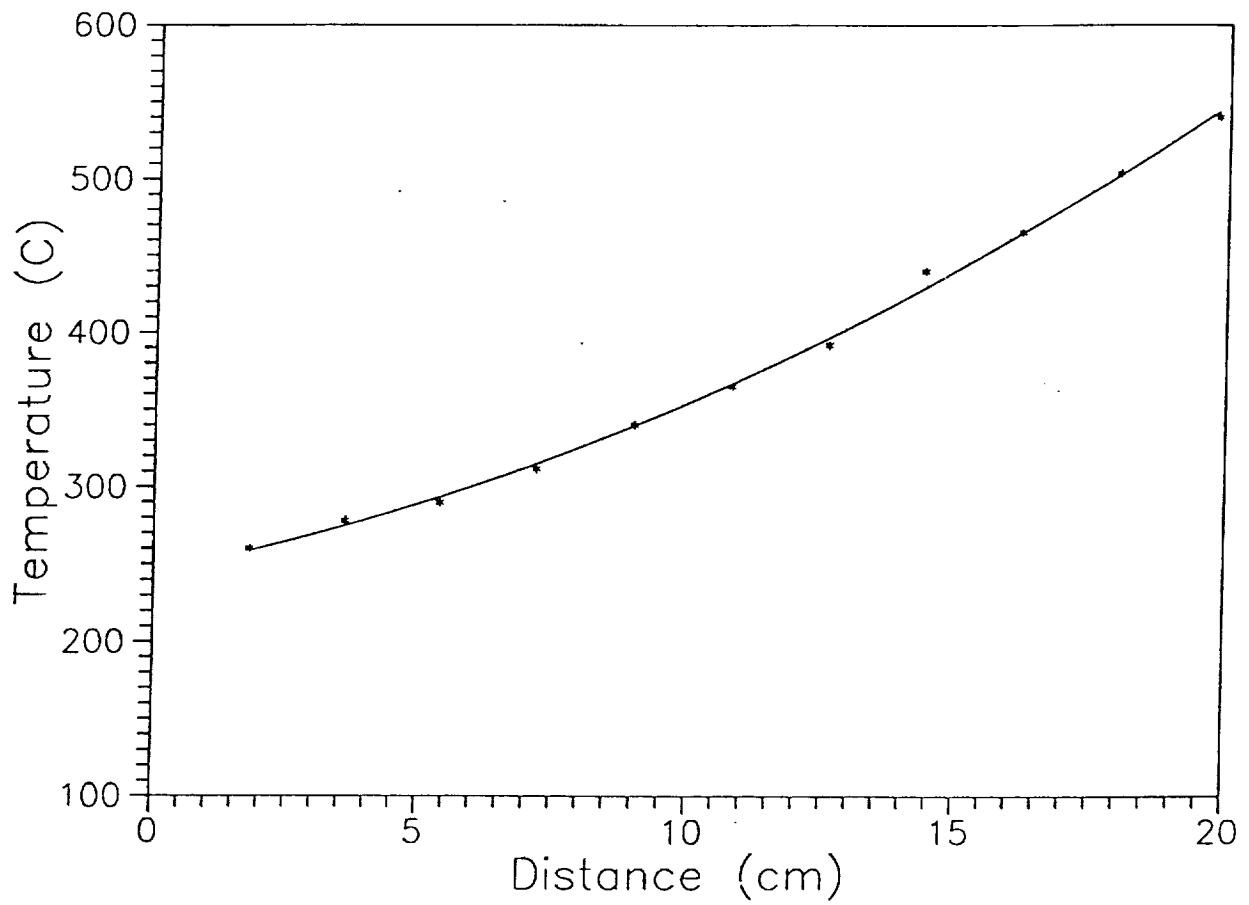
Figure 3.7: Experimentally determined temperature profile along the wall of the ampoule with a brass core fit by a second order polynomial. The equation of the line is $T = 0.4x^2 + 6.6x + 245$ where T is temperature in °C and x is distance in cm.
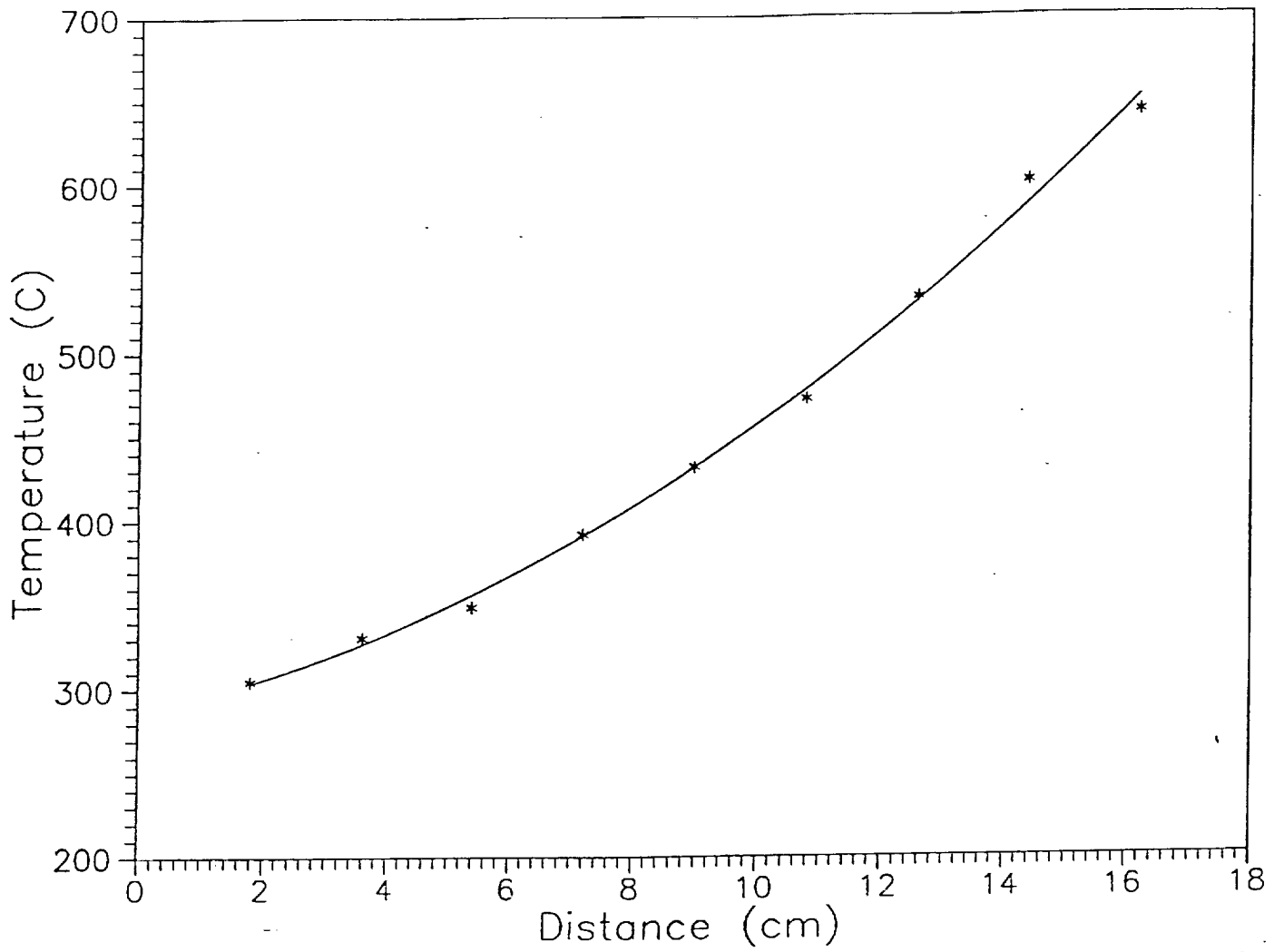
Figure 3.8: Experimentally determined temperature profile along the wall of the ampoule with a stainless steel core fit by a second order polynomial. The equation of the line is $T = 0.9x^2 + 8x + 286$ where T is temperature in °C and x is distance in cm.

3.2 Experimental Procedure

The experimental procedure was a series of processes:

- Material preparation

- Ampoule preparation

- Experiment

- Analysis

3.2.1 Material Preparation

Eutectic MnBi-Bi was solidified from 99.9999% pure Bi (Johnson Matthey Inc.) and 99.99% pure Mn (Aldrich Chemical Company Inc.). The MnBi-Bi eutectic composition is 0.71 ± 0.03 wt % Mn [60]. A balance with an accuracy of 0.1 mg was used to weigh 49.645 grams of Bi and 0.355 grams of Mn. The weighed Mn and Bi were loaded into a cleaned quartz ampoule and sealed under vacuum. The cleaning procedure is explained in the next section.

The material was homogenized in a rocking furnace. The temperature of the furnace was maintained at $650°$ C. The temperature of the rocking furnace was increased in steps of $30°$ C. The material was left in the furnace for 24 hours with alternate periods of rocking and no rocking. The furnace was then slowly cooled. The Mn-Bi was extracted from the ampoule by dissolving the quartz ampoule in HF. The extracted solid eutectic was etched with acetic acid and treated with acetone to remove any oxide layers. To test for homogeneity, samples of the material were taken and differential thermal analyses (DTA) were performed. All the samples had the same melting point, the eutectic melting point. The output graphs from the DTA are shown in figure 3.9 and figure 3.10. The solidified eutectic was ground to a powder with a clean mortar and pestle.

3.2.2 Ampoule preparation

As explained in the section on ampoule design, the tip of the ampoule had to be open because of the difficulty in getting the cleaning agents into the ampoule. The cleaning procedure involved allowing the fluids to run through the ampoule. First the ampoule was cleaned with Micro solution, a laboratory cleaner with the following ingredients: cations - sodium, ammonium, triethanolammonium; anions - ethylenediaminetetraacetate, linear alkyl sulfonates; nonions - polyethoxynonylphenol, water; manufactured by International Products Corporation. This was followed by running the following in turn through the ampoule: methanol, trichloroethane, acetone, methanol, HF and aqua regia. The ampoule was rinsed with deionized water after each chemical was run through it. A squirt bottle was used for forced rinsing. The ampoule was then fixed upside-down in a clamp and allowed to dry at room temperature. One end of the ampoule w... 'hen sealed with a blow torch. The ampoule was then evacuated and flushed with nitrogen. The blow torch was run up and down along the ampoule wall to evaporate any moisture still remaining in the ampoule. The powdered Mn-Bi was loaded into the ampoule. The loaded ampoule was evacuated. The material was allowed to sit in the vacuum for a few hours. The ampoule was backfilled with argon and flushed 2 or 3 times before sealing with a blow torch. Initially it was difficult to obtain good compaction of the material. On melting and resolidification the sample showed bubbles or gaps.

To prevent the formation of gaps the sample was melted in steps, each time pulling the ampoule out of the furnace and gently tapping to compact the material. To compact the material, about 2 cm of the ampoule was introduced into the furnace and allowed to melt. The ampoule was then withdrawn and tapped against the ground vertically. After the tapping, the ampoule was introduced into the furnace again. The second time about 4 cm of the ampoule was introduced into the furnace and allowed to melt and then the ampoule was withdrawn and tapped again. The above processes was repeated, each time melting a little more material, till all the material was melted.

34

3.2.3 Experiment

The furnace was allowed to attain a steady temperature profile. The hot end of the furnace was maintained at 700 or 750° C and the cold end was kept at 300° C. The prepared ampoule was left in the furnace for a set time. The ampoule was quenched by dropping it into a jar of cold water. The crystal was extracted by etching the quartz away with HF. The sample was analysed by atomic absorption spectroscopy, as described below.

One of the problems in the experiment was the formation of bubbles or gaps in the solidified material. The first 3 experiments showed many bubbles in the solidified material. A method of compacting was developed in order to try and minimize the bubbles. The compacting, as explained earlier in this chapter, was effective to a large exte.... The problem of the bubbles could not, however, be eliminated. Atleast 3 experiments showed bubbles even after the compacting. But all the other experiments done with the compacting did not show any bubbles.

3.2.4 Analysis

The quenched sample was cut into small pieces of measured lengths. A map of the sample was made so as to be able to locate the position of each piece. Each piece was weighed and dissolved in a standardized volume of 10 % nitric acid. Atomic absorption spectroscopy (AA) was done to determine the amount of Mn in the sample. The AA machine used was a Perkin-Elmer model 5000. A schematic of the machine is shown in figure 3.11, and figure 3.12 shows a photograph of the machine. The Perkin Elmer Zeeman 5000 is a microprocessor-controlled atomic absorption spectrophotometer. All the mechanical, electrical and optical functions of the instrument are electronically controlled and activated, enabling the analytical conditions to be set either manually via the keyboard, or from preprogrammed magnetic cards. Analytical conditions are entered using keyboards. Each control parameter has a separate key, which is used to assemble the analysis program. The completed program can be saved and recalled later. Recalling a program automatically resets the instrument parameters to the

desired values.

A number of publications give a general background on the principles of operating an atomic absorption instrument [61, 62]. The Perkin Elmer manual lists a number of analytical techniques. The conditions and parameters used for our analysis were taken from the manual. In all the analyses, the flame aspirator with the impact bead flow modifier was employed. Manganese lamp for the Zeeman 5000 was purchased from Perkin Elmer. All the labware was scrupulously cleaned and labeled to ensure that no contamination took place. All glassware was acid washed and rinsed in distilled water before use.

The AA manual specifies the following parameters for Mn:

- Wavelength: 279.8 A

- Slit height: 0.2 nm

- Flame: Acetylene-air

- Modifier: 0.2 % calcium chloride in 1 % hydrochloric acid

- Linear range: 2 - 20 parts per million (ppm)

A set of solutions was used for adjusting and calibrating the AA unit. The standards were made by diluting stock manganese solutions made especially for AA work. The stock solutions come in a matrix (concentration of companion ions and acids resulting from dissolving the elemental salts used to manufacture the standard). The stock solutions were purchased from Fisher Scientific.

3.2.5 Sample Preparation

The samples were digested in a beaker with 5 ml of concentrated nitric acid. The digested samples were diluted to a concentration within the linear absorbance range for the element. Dilution was accomplished by adding a modifier solution as indicated by the Zeeman 5000 manual. The diluted sample was transferred to a Nalgene bottle and held for analysis. At the same time a blank solution (without any sample in it)

36

was also prepared. The blank was used as a reference to zero the machine before calibrating.

The AA machine was calibrated by using standard solutions. The absorbance of the standard solutions was used to set concentration to read out directly on the AA spectometer. Each piece of the sample was prepared for analysis in a calculated volume. The obtained Mn concentration was converted to mass fraction Mn in the solid. The results are shown in the next chapter.

Chapter 4

Results and Discussion

The experiments were carried out in the furnace with a stainless steel core, as explained in the preceeding chapter. The temperature profiles along the wall of the ampoule were shown in the preceeding chapter. The samples were analysed by atomic absorption spectrophotometry to determine the amount of Mn along the length of the sample. The concentration of Mn was plotted against distance. A summary of the experiments is presented in table 4.1.

The following figures show the results obtained from the analyses of the samples. In all the figures the right side was the upper hot end. Comparison of theoretical and experimental data was done in nondimensional units. The data were nondimensionalized by using the following definitions: relative distance = x/total length of solidified sample; relative concentration = actual Concentration/initial concentration. The initial concentration was determined by analysing a piece of the initially homogenized material each time along with the experimental specimen. The initial concentration for the different experiments was in the range of 0.65 to 0.72 wt % Mn (eutectic concentration = 0.71 ± 0.03 wt % Mn). Some results from the theoretical modeling are shown in appendix B.

Figure 4.1 shows results from the 3 hour experiment. It can be seen that there was one piece near the hot end that was much higher in Mn concentration than the rest of the pieces. The observed concentration profile was not as expected. In order

PRECEDING PAGE BLANK NOT FILMED

Exp. No.	Time	Results
1	2 Days	Analysis showed large conc. change over length of ampoule.
2	5 Days	Conc. gradient smaller than experiment 1.
3	10 Days	Conc. profile looks like that predicted by theory.
4	15 Days	Conc. gradient more like that predicted by theory.
5	20 Days	On quenching, found bubbles along the length of sample.
6	6 Days	Conc. profile similar to 5 day experiment.
7	15 seconds	Almost constant concentration along the length of sample.
8	1 Day	On quenching found bubbles along the length of the sample.
9	2 Days	Similar to experiment 1.
10	2 Days	Similar to experiments 1 and 9
11	5 Days	Similar to experiment 2.
12	6 Days	Similar to experiment 6.
13	3 Hours	Very large conc. change. Most of the Mn at the top of ampoule.
14	3 Hours	Similar to experiment 13.
15	10 Hours	Analysis showed concentration change over length of ampoule.

Table 4.1: A summary of the experiments conducted in the laboratory.

to determine if the point in question was an error in experiment or a true phenomenon, the experiment was repeated. Figure 4.2 shows that the second 3 hour experiment produced results similar to the first 3 hour experiment. Since the experiment showed similar results when repeated, it could be said that the high concentration of Mn observed near the hot end was not due to an experimental error.

Figures 4.3 and 4.4 show results from the 2 day experiments. Both the graphs show a similar trend. The concentration of Mn was high at the hot end of the furnace. The high concentration at the hot end was not expected, but since all the 2 day experiments showed similar results it apparently was a real phenomenon.

Figures 4.6-4.9 show the results from 5, 6, 10, and 15 day experiments. The concentration profiles obtained in these experiments show a trend. The concentration of Mn at the cold end was small. The concentration rose towards the middle of the furnace and then fell a little before rising again. The experiments were repeated in order to confirm the observed concentration changes. Figure 4.10 shows the results from another 5 day experiment.
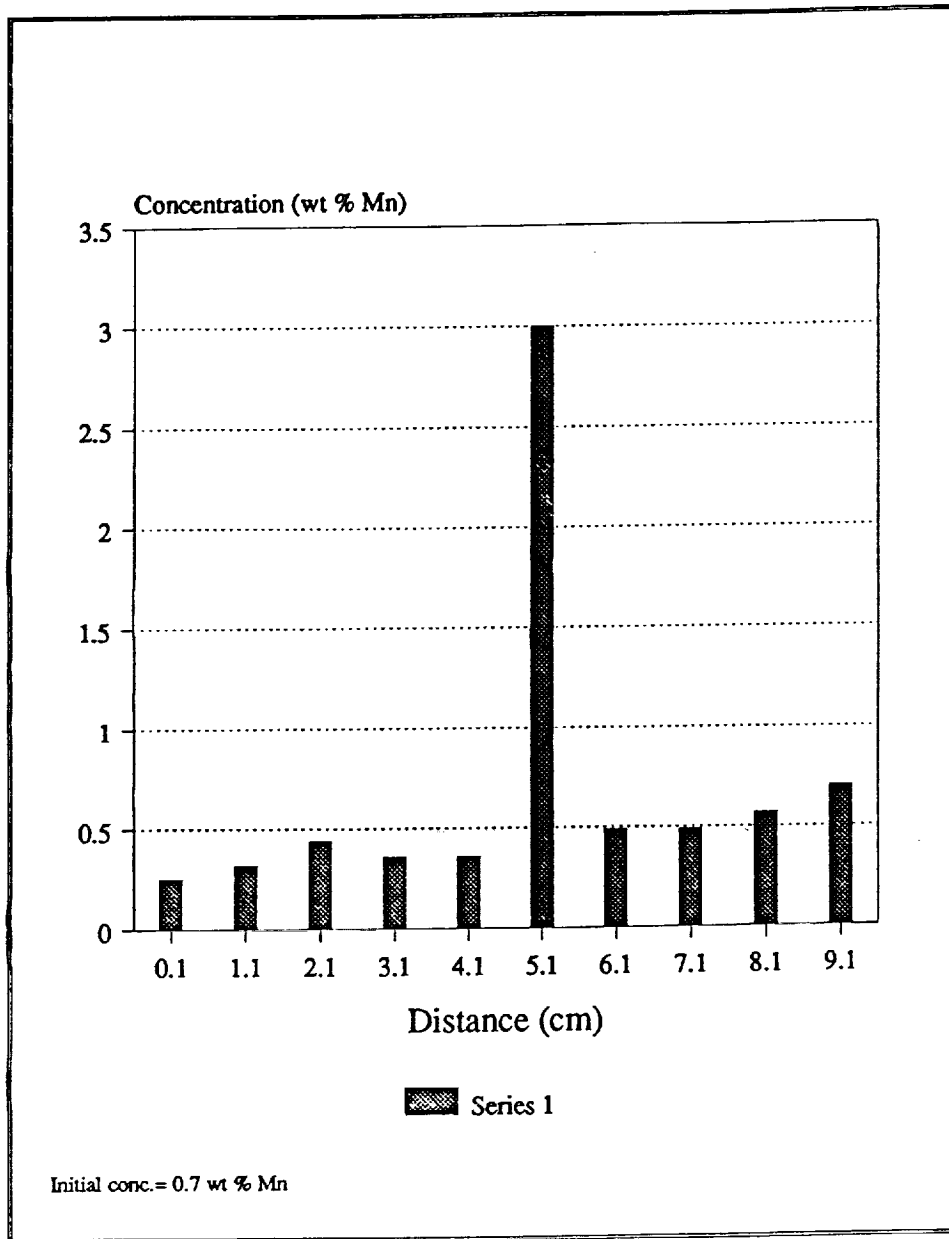
Figure 4.1: Experiment no. 13: Concentration of Mn along the length of a sample after 3 hours.
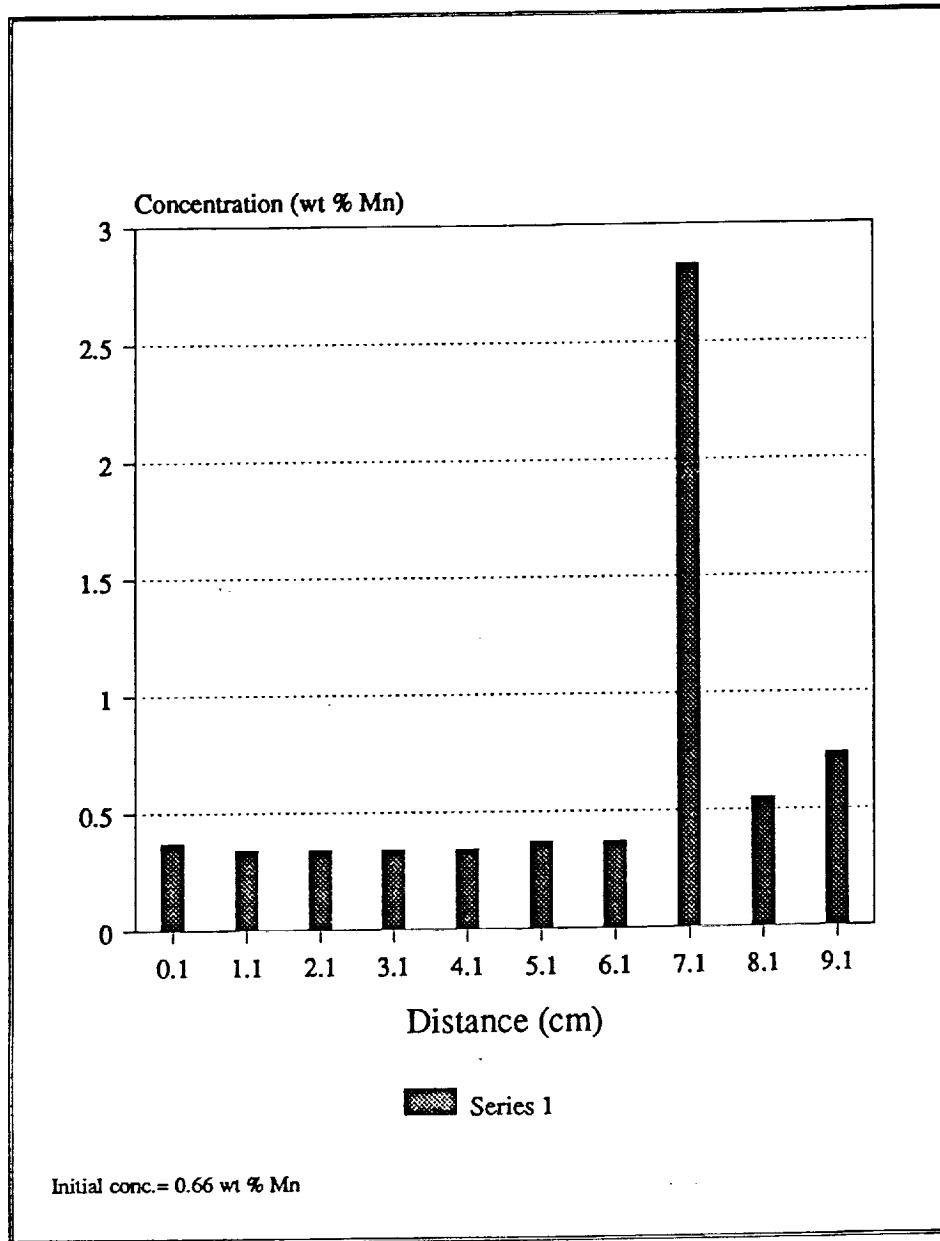
Figure 4.2: Experiment no. 14: Concentration of Mn along the length of a sample -
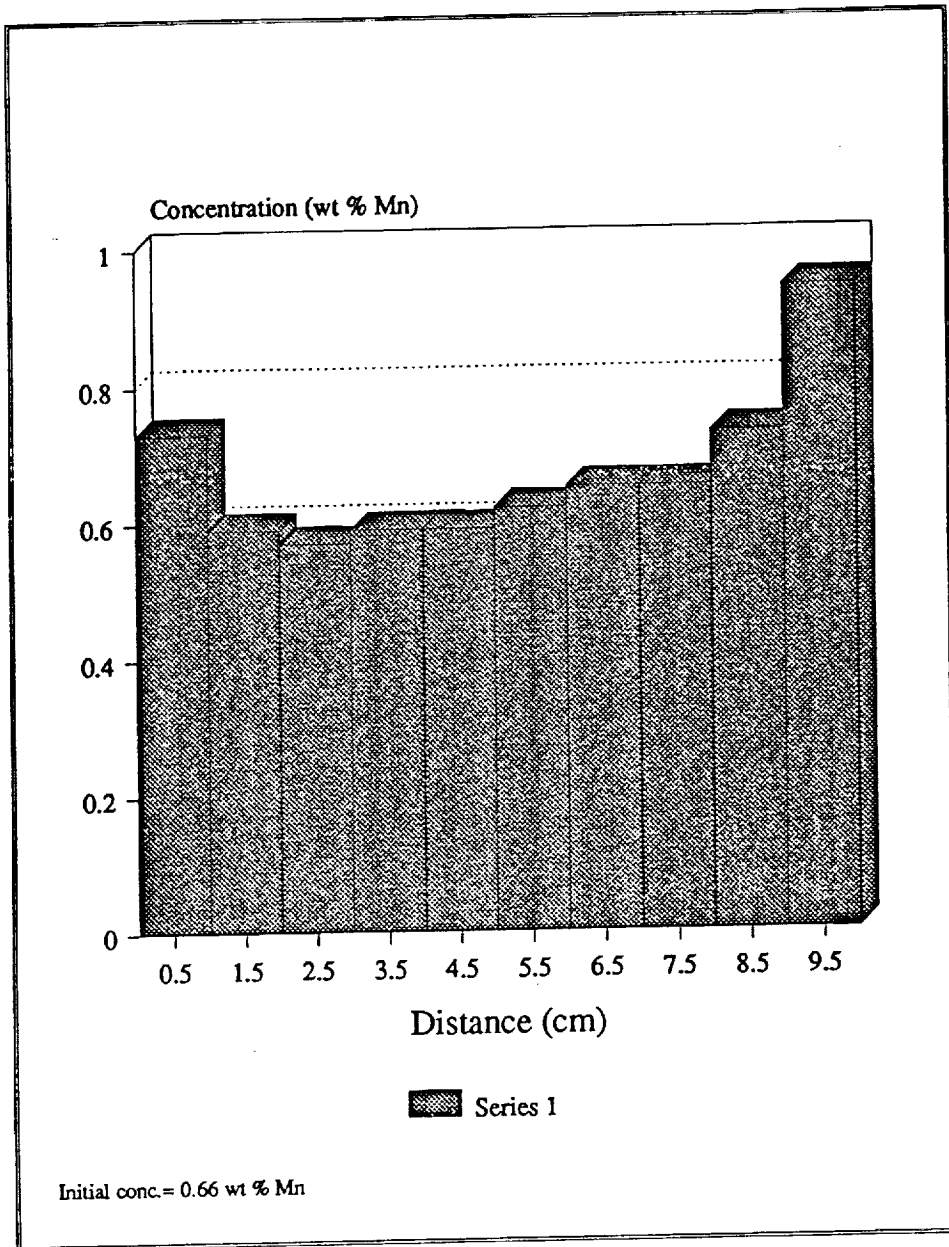another 3 hour experiment.

Figure 4.3: Experiment no. 1: Concentration of Mn along the length of a sample after a 2 day experiment.
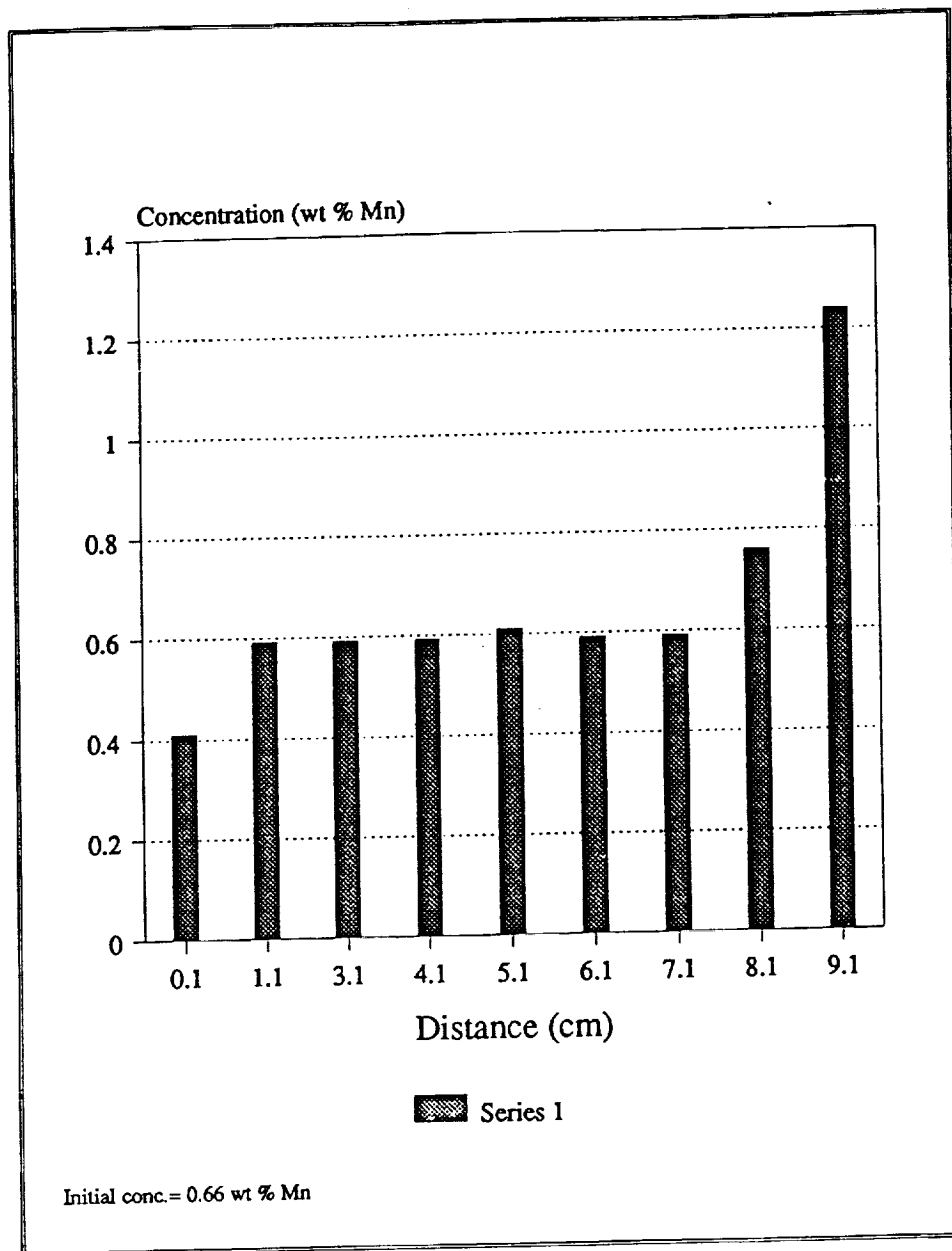
Figure 4.4: Experiment no. 9: Concentration of Mn along the length of a sample after a 2 day experiment.
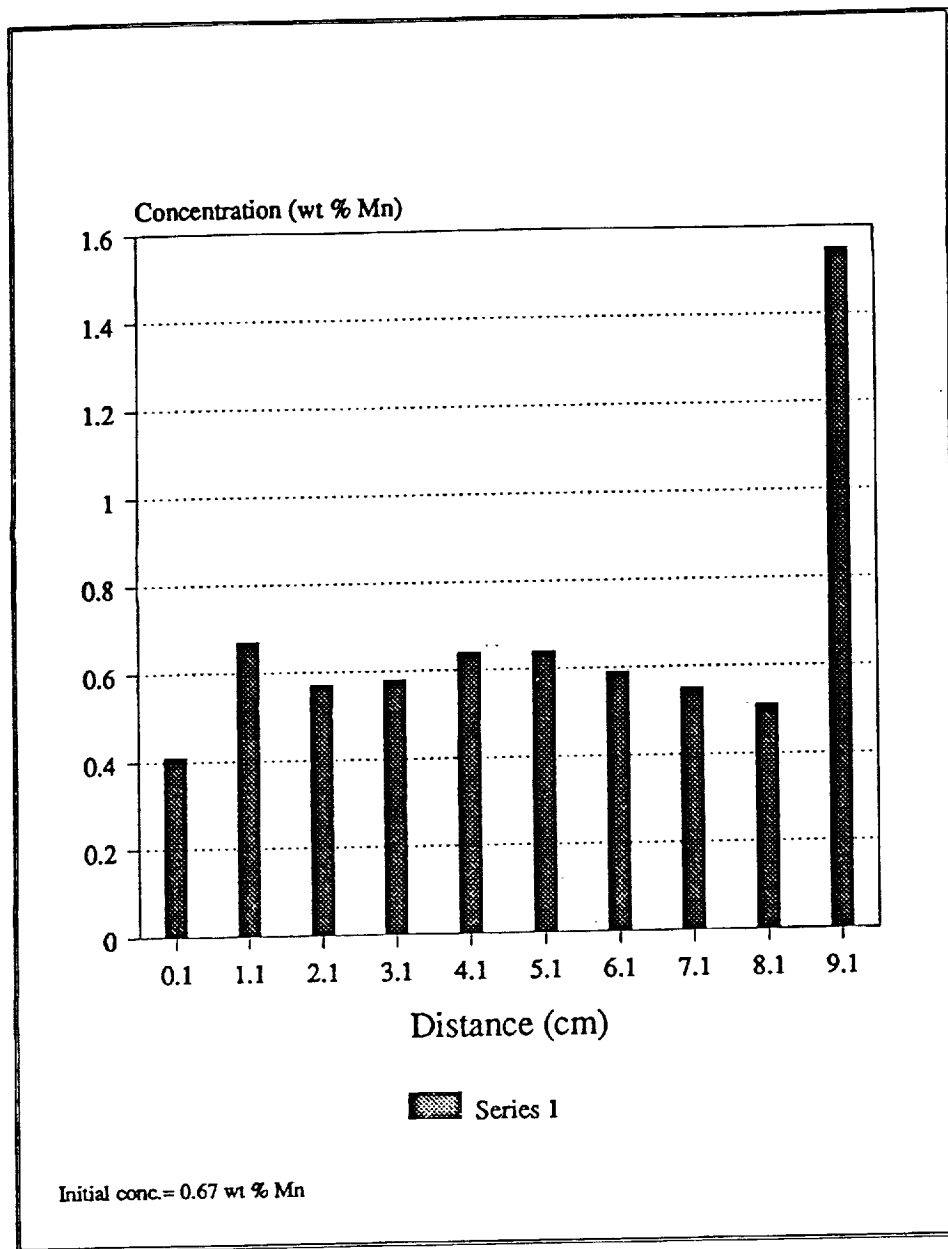
Figure 4.5: Experiment no. 10: Concentration of Mn along the length of a sample -third 2 day experiment.

Figure 4.6: Experiment no.2: Concentration of Mn along the length of a sample after a 5 day experiment.

Concentration (wt % Mn)

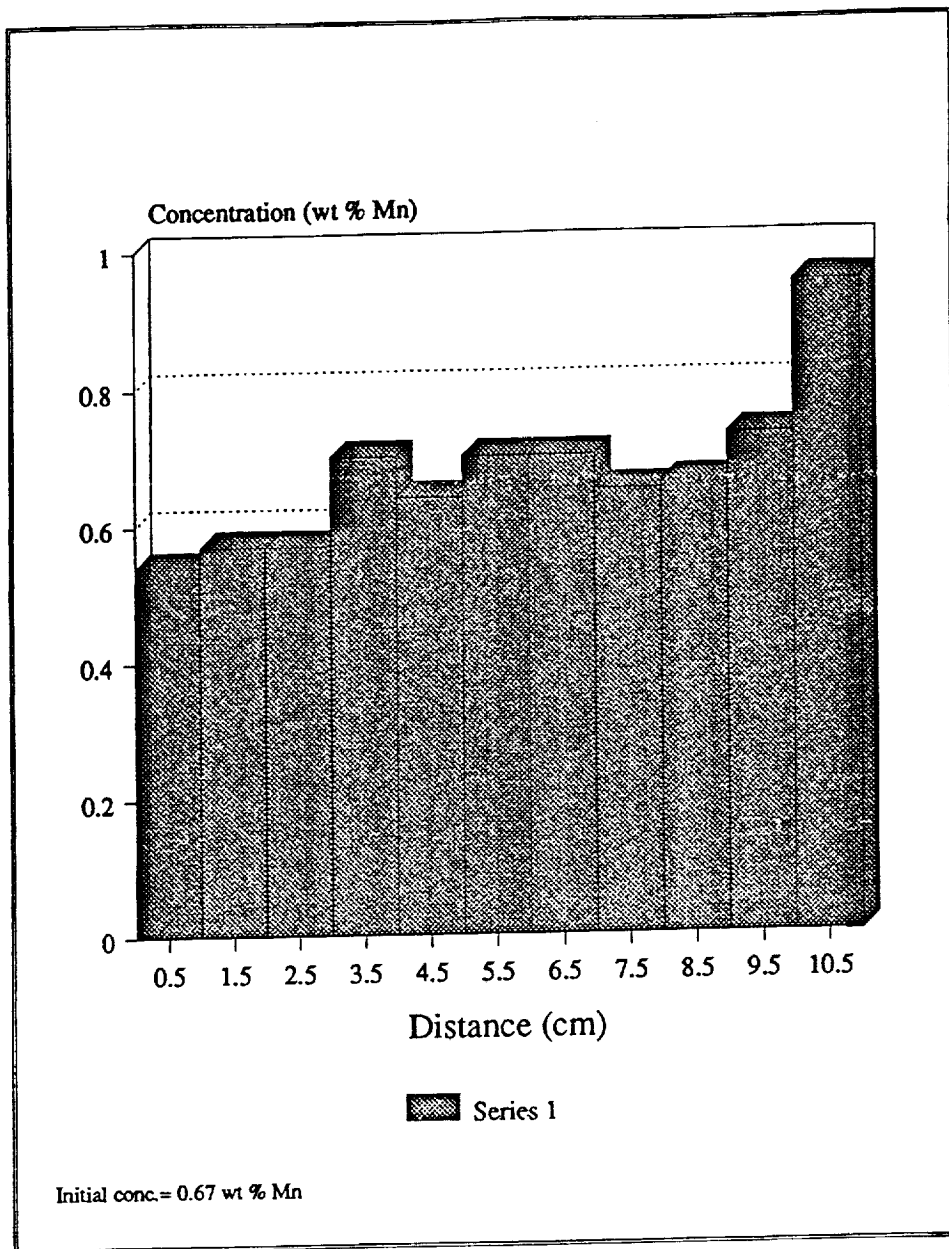**Distance (cm)**

Series 1

Initial conc. 0.72 wt % Mn

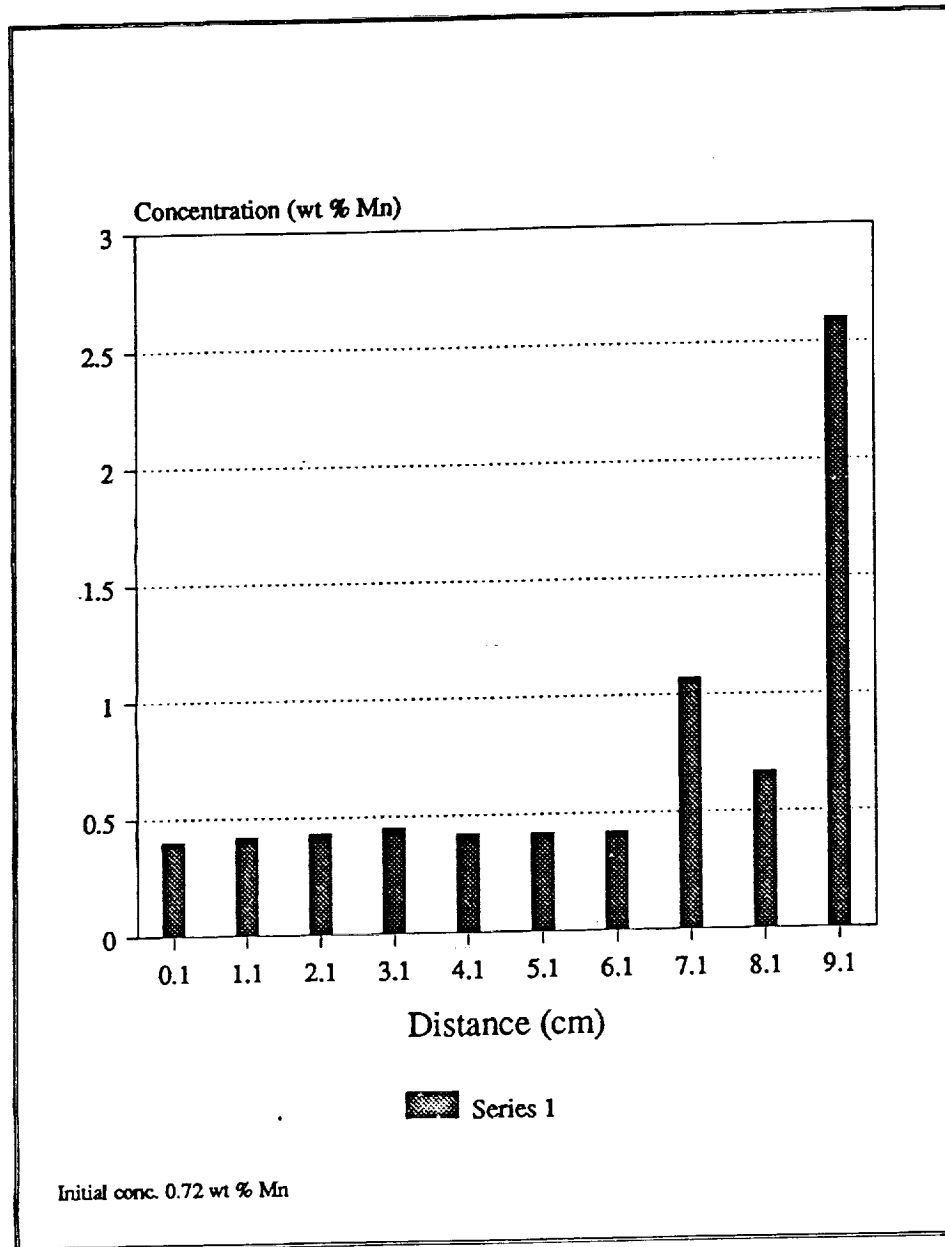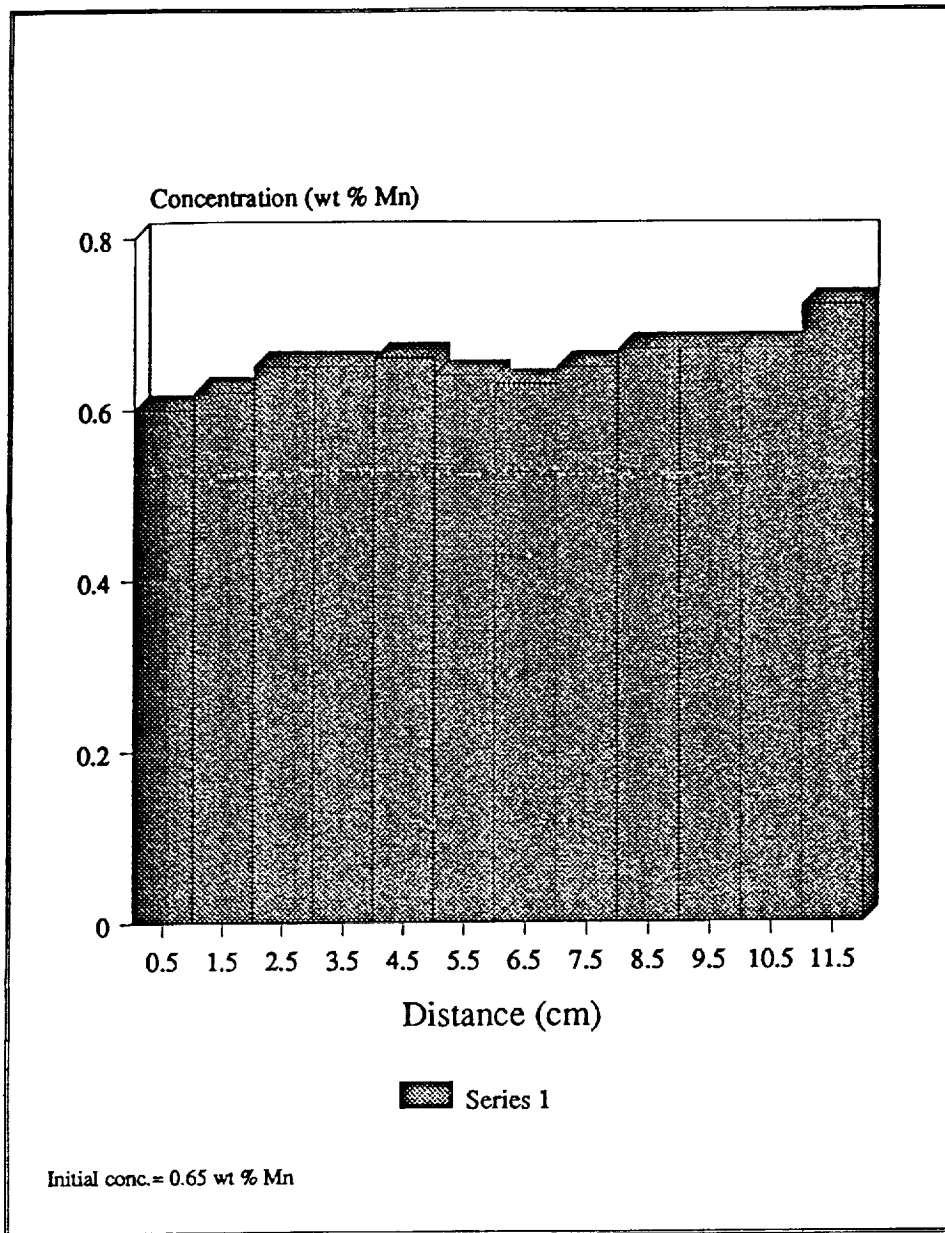Figure 4.7: Experiment no.6: Concentration of Mn along the length of a sample after a 6 day experiment.

Figure 4.8: Experiment no.3: Concentration of Mn along the length of a sample after a 10 day experiment.
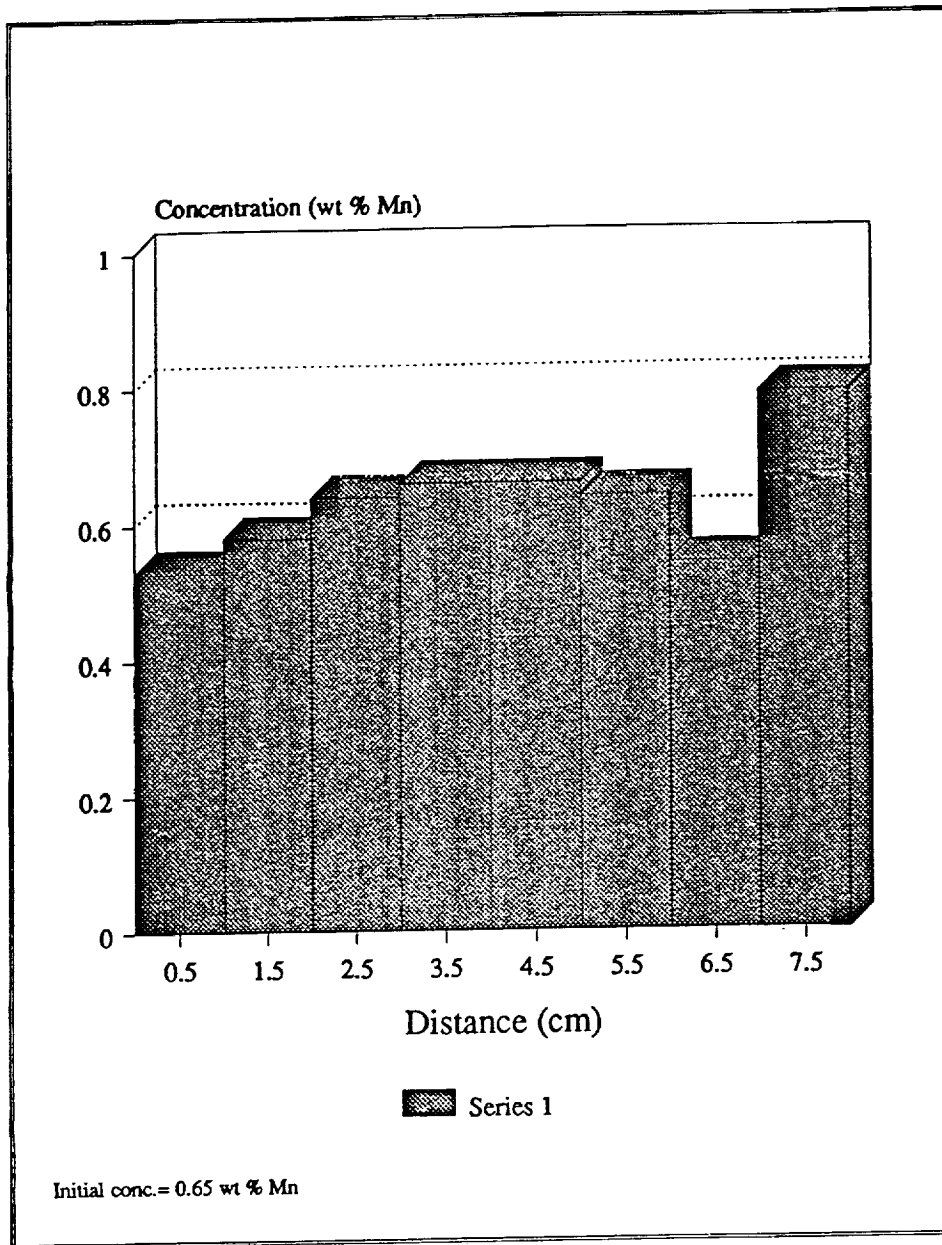
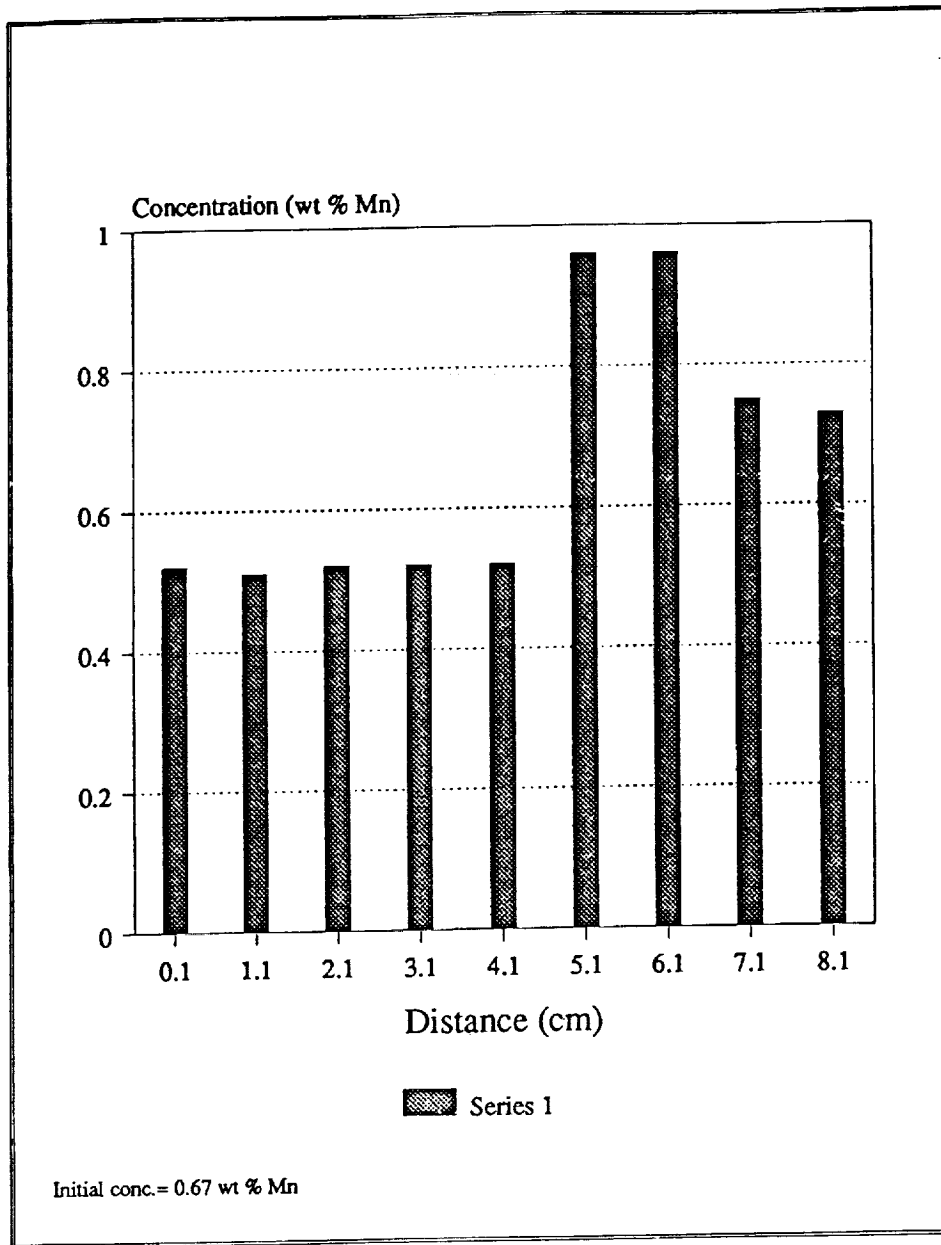Figure 4.9: Experiment no.4: Concentration of Mn along the length of a sample- 15 day experiment.

Figure 4.10: Experiment no.11: Concentration of Mn along the length of a sample -second 5 day experiment.

The analytical solution for constant temperature gradient (appendix A) requires very little computer time to produce a concentration profile. Figure 4.12 shows a three dimensional plot of concentration versus time and distance for a Soret coefficient of $10^{-7} cm^2/°C.s$ from the analytical solution (equation A.19). The initial concentration was assumed to be homogeneous. The concentration at time equals zero should be unity in figure 4.12, but the concentration actually deviates a little from 1 because the exact analytical solution has infinite terms and the calculation done to generate figure 4.12 includes only 100 terms. The finite difference solution (appendix A) involved more computation and typically required about 1 hour of CPU time on the gould (mainframe) system for a grid of 1000 points. The finite difference solution can be used for variable temperature gradient, variable physical properties and non-homogeneous initial conditions. A comparison of the finite difference and analytical solutions is given in appendix A. The figures in the appendix show that the analytical and numerical solutions agree very well.

Figure 4.11 shows the results obtained from a constant temperature experiment. The material was kept in an isothermal furnace at 330 °C for 10 hours. There was a change in the concentration profile with a large amount of Mn being at the top (hot) end of the furnace. These results are not as expected for a homogeneous melt kept at a constant temperature. The constant temperature results support the idea that there was some effect which changed the concentration profile in the system initially.
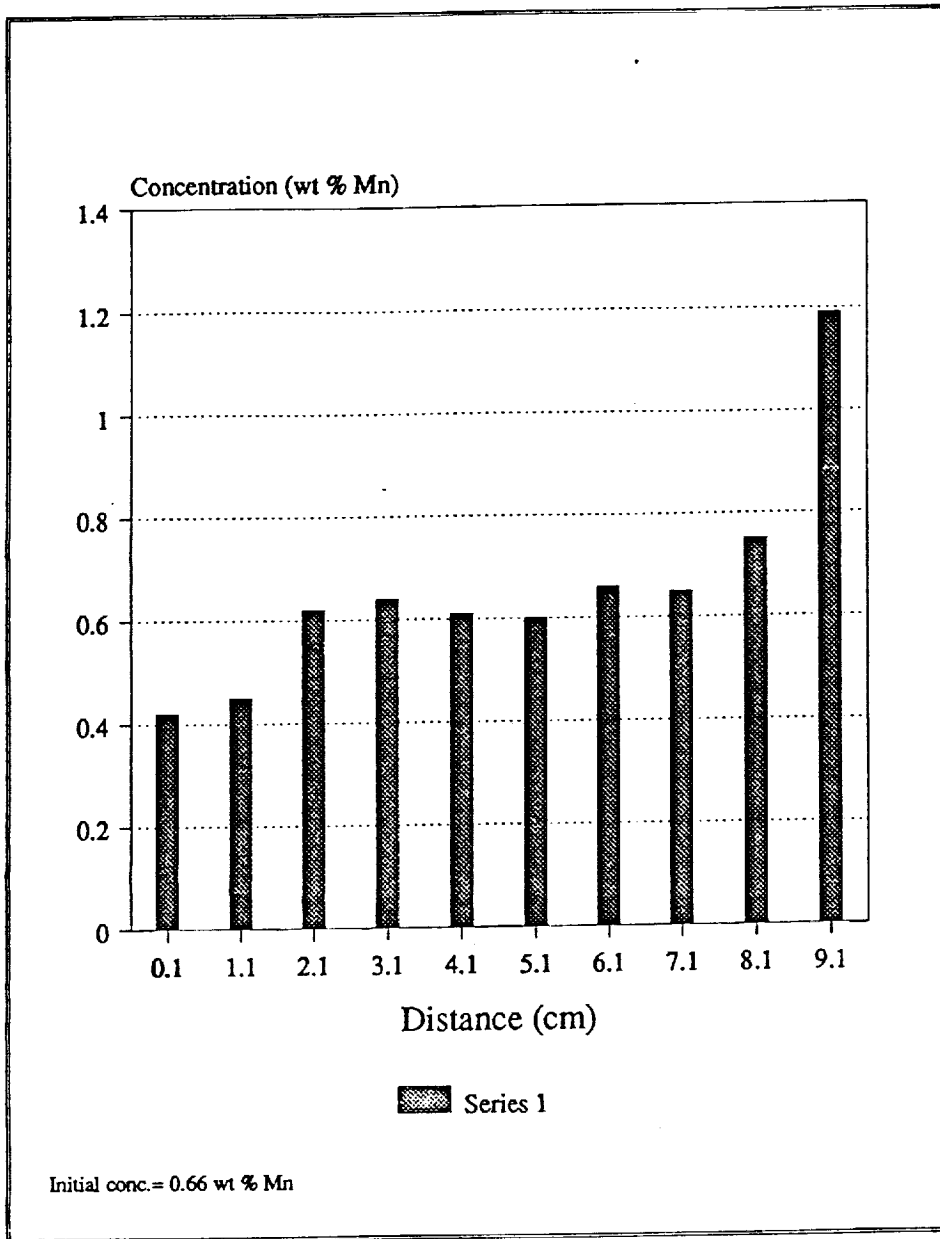
Figure 4.11: Experiment no. 15: Concentration of Mn along the length of a sample after a 10 hour experiment with a constant temperature of 330 °C.
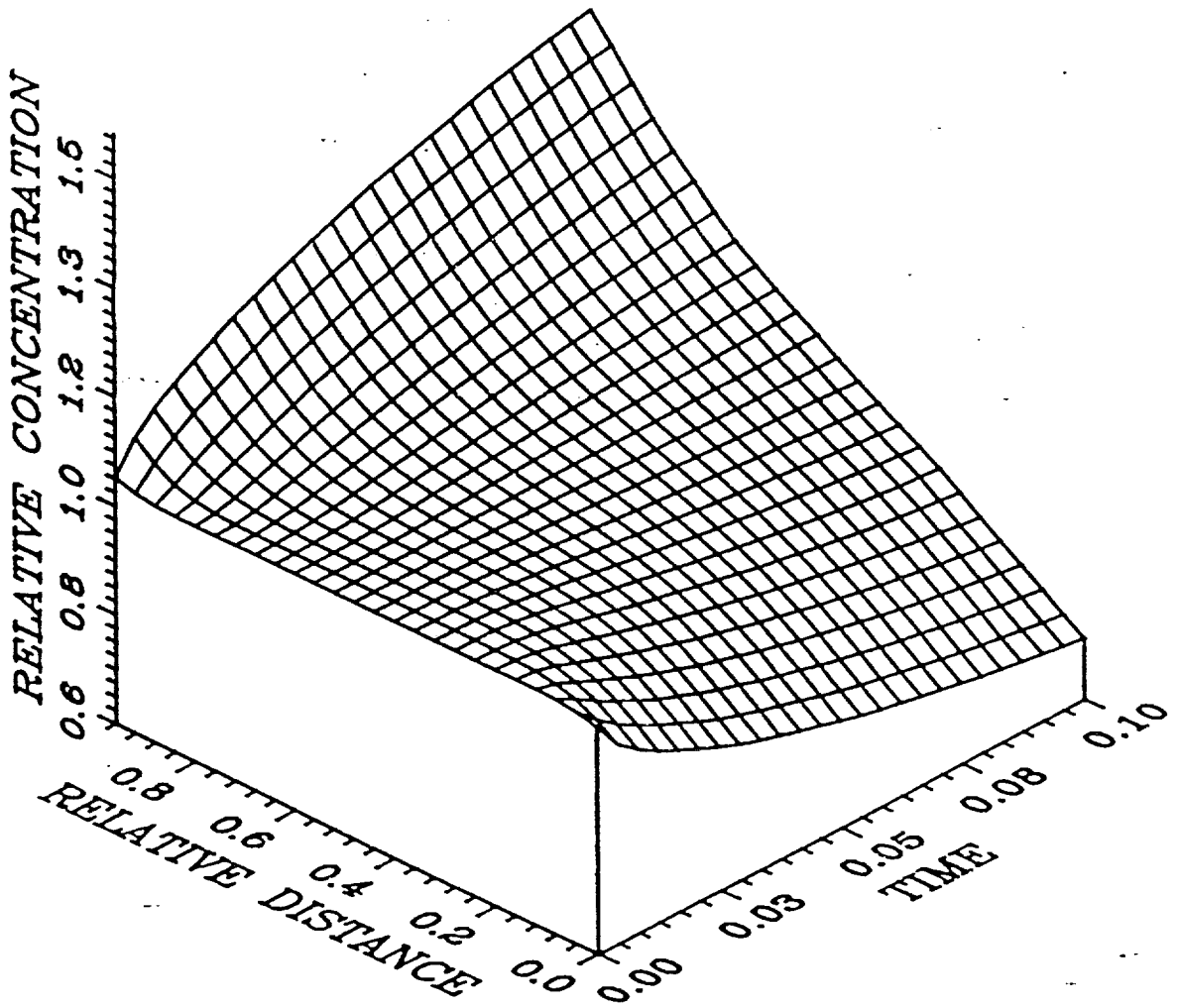
Figure 4.12: Results from the analytical solution for Soret coefficient $= 10^{-7}$ cm^2/°C.s, $D = 10^{-5}$ cm^2/s and homogeneous initial conditions. Here time is dimensionless time $\zeta = tD/L^2$; where t = time in seconds, D = diffusion coefficient, L = length of sample in cm.

Figure 4.13: Relative concentration as a function of relative distance in a molten binary alloy: Theoretical curves were calculated using t = 8 days i.e. dimensionless time $\zeta = 69.12 \times 10^{-3}$, G = actual temperature profile, $D = 10^{-5} cm^2/s$; initial condition taken from the 2 day experiment.

Figure 4.14: Relative concentration as a function of relative distance in a molten binary alloy: Theoretical curves were calculated using t = 13 days i.e. dimensionless time $\zeta = 112.32 \times 10^{-3}$, G = actual temperature profile, $D = 10^{-5} cm^2/s$; initial condition taken from the 2 day experiment.

Figure 4.15: Relative concentration as a function of relative distance in a molten binary alloy: Theoretical curves were calculated using t = 10 days i.e. dimensionless time $\zeta = 69.12 \times 10^{-3}$, G = actual temperature profile, $D = 10^{-5} cm^2/s$; starting with homogeneous initial conditions.
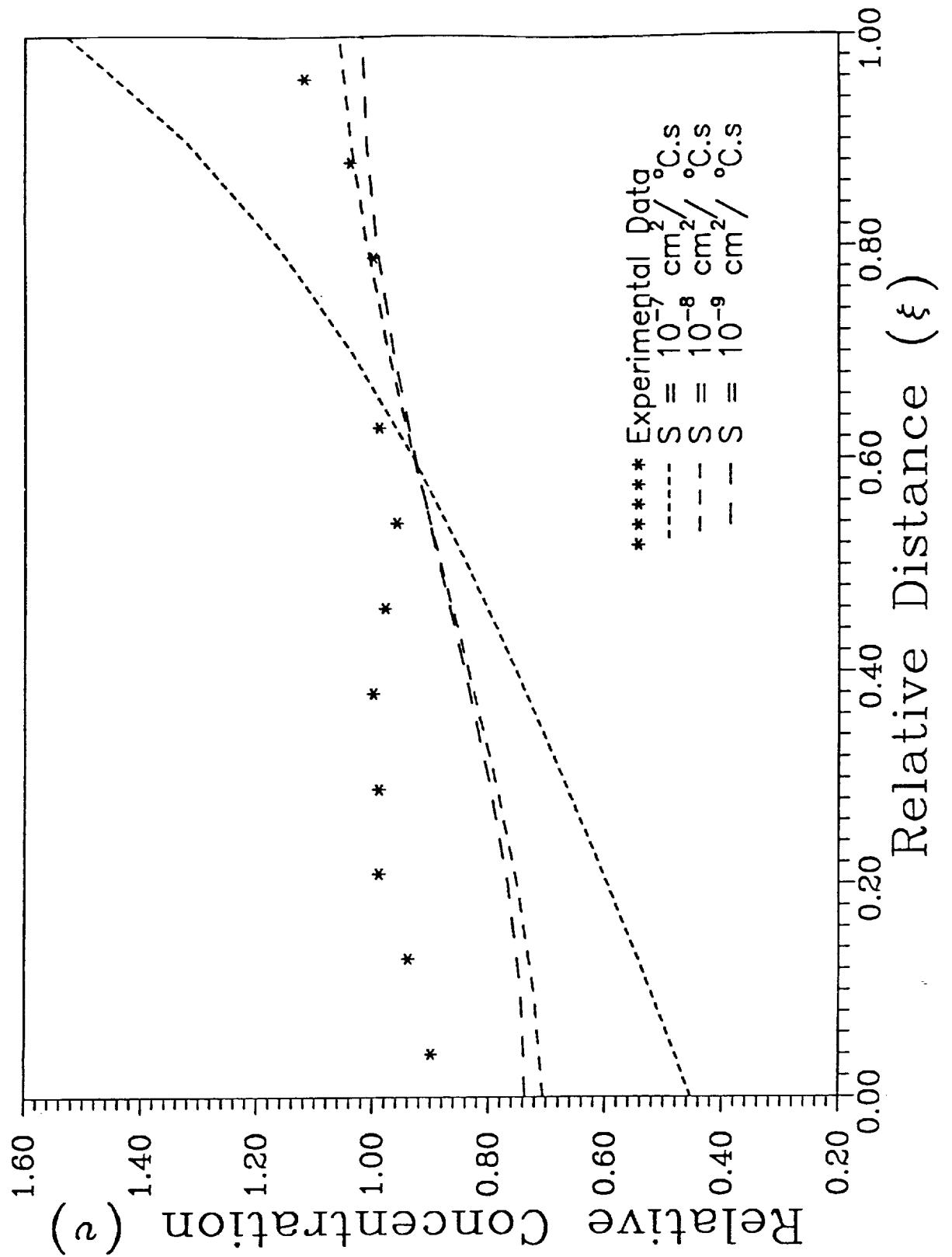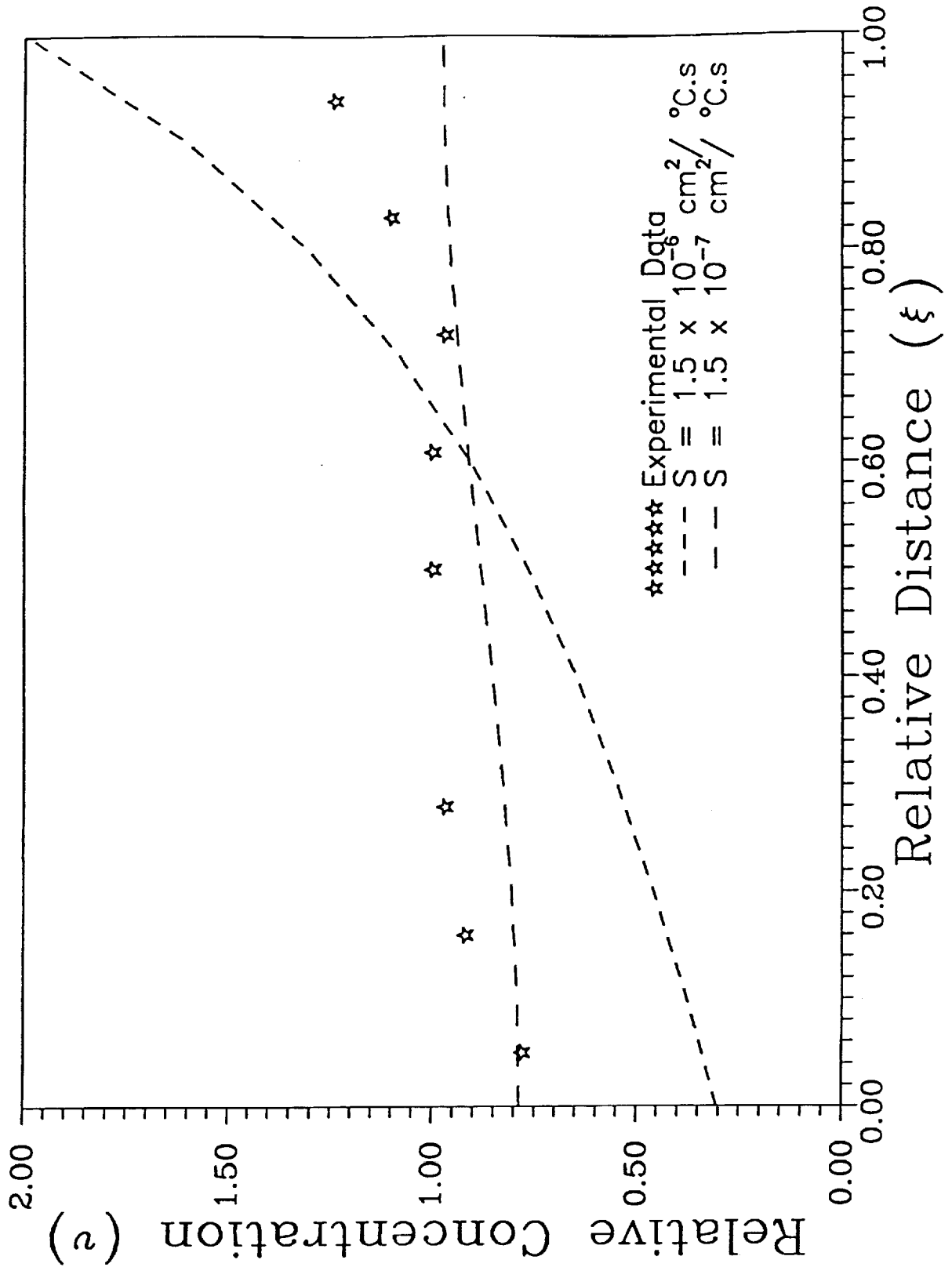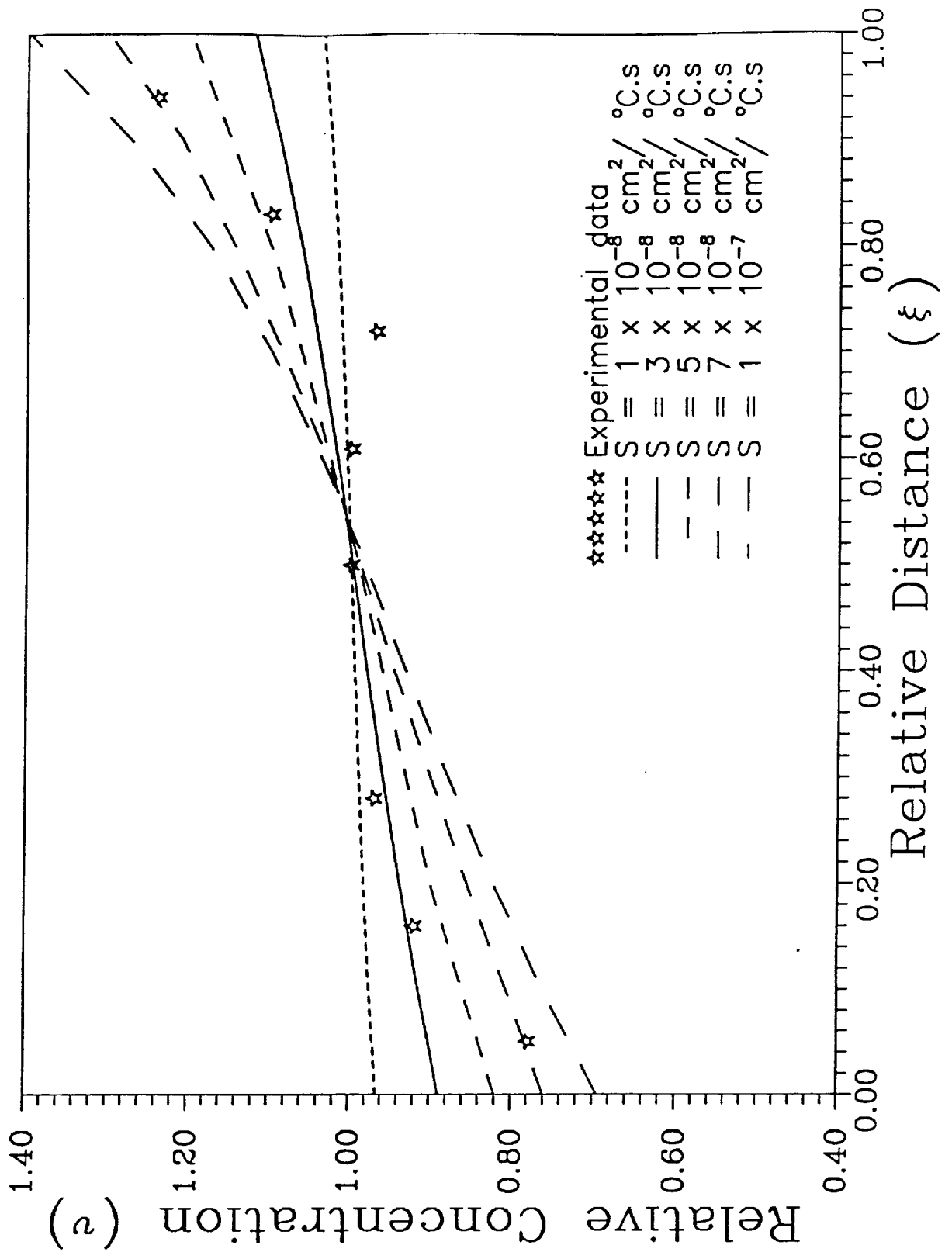
Figure 4.16: Relative concentration as a function of relative distance in a molten binary alloy: Theoretical curves were calculated using t = 15 days i.e. dimensionless time $\zeta = 112.32 \times 10^{-3}$, G = actual temperature profile, $D = 10^{-5} cm^2/s$; starting from homogeneous initial conditions.

The results obtained for the 3 hour and the 2 day experiments are difficult to explain. The theoretical curves generated by using different values of S both for homogeneous initial condition and for initial condition taken from the results of a 2 day experiment (experiment 9) suggest that there should not have been much change in the concentration profile in 3 hours. The theoretical curves for different Soret coefficients are presented in figures 4.12-15. For the given conditions we should have observed an almost constant concentration in the 3 hour experiment. Also from the theoretical concentration profiles it is seen that the Soret effect should not have induced a very large concentration change in 2 days.

One possible explanation for the 3 hour and the 2 day experiments is that there was gravitational settling initially in the melt, since the density of liquid Bi (10.4 g/cc [66]) is much higher than Mn (6.3 g/cc [66]). If the two components of the sample did not melt at exactly the same rate, it is possible that as the sample was melted Bi moved downwards while Mn moved upwards.

The isothermal experiment was conducted in order to determine if the system would show any changes in the absence of Soret effect. For a constant temperature there should be no change in the concentration profile. The results (figure 4.11) show that the melt concentration changed from homogeneous conditions very quickly. Hence the theoretical calculations done assuming an initial homogeneous condition cannot be accurate, at least for short times. The constant temperature results confirmed that there was some effect which changed the concentration profile in the system initially. A better comparison of the experimental and theoretical results might be possible using the results from a short experiment as the initial concentration for theoretical calculations.

All of the theoretical results in appendix A were obtained assuming an initially homogeneous condition. Figure 4.15 shows the results from a finite difference computation with the initial condition being the results obtained in a 2 day

62

experiment (experiment no. 9). The stepped concentration profile shown in figure 4.4 was used as the initial condition for figure 4.15 and figure 4.16. In the figures, the curves were generated for 8 days and 13 days using results of the 2 day experiment as an initial condition, such that the total time corresponding to the experiments are 10 days and 15 days respectively. Figure 4.15 shows results for $\zeta = 69.12 \times 10^{-3}$ and figure 4.16 shows results for $\zeta = 112.32 \times 10^{-3}$. Comparison of the theoretical curves with the experimental data does not show good agreement.

The concentration profiles of the experiments run for 10 and 15 days, when compared to the theoretical curves calculated assuming homogeneous initial conditions, agree with the theoretical predictions better than the shorter experiments. The results obtained would support the idea that the system initially experienced some gravity effects. The experimental curves from the long time experiments were similar to the theoretical curves but showed a larger maximum and smaller minimum value than that predicted by theory. The concentration gradients of the experimental curves are much larger, at the two ends of the sample, than that predicted by theory.

By comparing the experimental concentration profiles to the theoretical concentration profiles with homogeneous initial conditions, a rough estimate of the Soret coefficient can be made. A comparison of the experimental data to the theoretical data was made assuming a diffusion coefficient of 1×10^{-5} cm^2/s. The magnitude of this diffusion coefficient is typical of those for liquid metals in the given temperature range. The comparison showed that the trend of the experimental data was similar to that predicted by theory, except in the middle of the sample. In the middle of the sample the measured concentration showed a decrease and then increased towards the hotter end. From the theoretical concentration profile it was expected that the concentration in the middle of the sample would be constant or increasing. From the comparison it would appear that the Soret coefficient is in the range of 1 - $5 \times 10^{-8} cm^2/s^\circ C$.

4.2   Conclusions

The experiments performed in the lab and the theoretical modeling give rise to the following conclusions:

1. The Soret effect was observed in the Mn-Bi samples. The experimental results did not match the theoretical predictions for short time periods. But when samples were kept in the temperature gradient for 10 or more days, the results were similar to those predicted by theory.

2. A comparison of the theoretically obtained concentration profiles to those obtained by experiment shows that the experimental results matched the theoretical results better as time increased, i.e. when the material was kept in the temperature gradient for longer periods of time, the concentration profile obtained was more like that predicted by theory. From the comparision of theoretical and experimental data it can be said that the Soret coefficient is in the range $1 - 5 \times 10^{-8} cm^2/°C.s.$

3. The shorter experiments, 3 hours and 2 days, showed unexpected concentration profiles. For the 3 hour experiment it was expected that the concentration would be almost constant along the length of the sample. But both the 3 hour experiments showed a peak in the Mn concentration close to the hot end (top end) of the furnace. The 2 day experiments showed a trend somewhat like that predicted by theory, but still seemed to have a higher concentration of Mn towards the hot end. It is possible that initially there was some gravity effect. If both the elements of the sample did not melt at the same time, Bi being much more dense than Mn would move downwards. Also since the sample was compacted by melting in stages and tapping the ampoule, any settling effects would be affected.

4. The experimental curves for the longer time experiments were similar to the theoretical curves, but showed a much larger maximum and much smaller minimum concentration than that predicted by theory.

5. The constant temperature experiment supported the idea that there was some effect in the system which changed the concentration in the early stages of the

65

experiment. When the results from the 2 day experiment were used as the initial condition in the theoretical model, the results showed a better agreement between theory and experiment.

6. The separation caused by thermotransport is dissipated by convective motion of the fluid. Since there is no convection is space, the ideal place for the thermal diffusion experiments would be in space in a microgravity environment.

APPENDIX C

EFFECT OF CONVECTION ON THE MICROSTRUCTURE OF MnBi/Bi EUTECTIC GROWING WITH A STEPPED INTERFACE

JAYSHREE SETH

SUMMARY

The objective of this project is to develop a numerical model to study the influence of convective flow on the microstructure of MnBi/Bi lamellar eutectic when one phase projects out into the melt creating a stepped interface.

To investigate the effect of convection on a stepped interface, and compare the results with that obtained for a planar interface, a theoretical model was formulated. The computational domain, the governing differential equations and the existing boundary conditions for the velocity and the concentration field were identified. The velocity field generated due to the flow of melt over the steps was solved numerically. A numerical scheme based on a finite difference approach was developed for solving the concentration field.

A. INTRODUCTION

The primary motivation for this work arises from experiments on solidification in the reduced gravity environment of space. These showed marked structural difference from identically processed earth grown samples. The difference has been attributed to the absence of convective currents at low g as compared to conditions on earth.

Baskaran [1] developed a two dimensional model to study the effect of convection on the lamellar spacing of MnBi/Bi eutectic. Eisa [2] performed theoretical work using the numerical results for the convection field with more intense convection and developed a correlation for the effect of convection on the interfacial undercooling. Chandrasekhar [3] performed numerical analysis to study the effect of convection on the rod spacing. Caram [4] developed a developed a three dimensional numerical model for the influence of convection on the eutectic microstructure. Chandrasekhar [3] performed decantation experiments wherein the remaining melt was poured off during the solidification of the MnBi/Bi eutectic. He found that the MnBi fibers were projecting ahead of the Bi matrix, which implied that the interface was not planar. In the present work a lamellar structure is being studied rather than a rod structure for computational ease; the diffusional domain of a lamellar eutectic is two dimensional rather than three dimensional as in the case of a rod eutectic. The resulting observations are expected to hold for a rod structure in a semi-quantative sense.

B. PROGRESS

Given below is the development of the model, the assumptions that were made and the numerical scheme based on a finite difference approach.

1. THEORETICAL MODEL

In order to predict the effect of various phenomena, convection in particular, on the eutectic microstructure, it is imperative that the compositional field ahead of the growing interface be known accurately. As the adjacent phases of the binary eutectic grow, atoms are rejected into the melt due to partitioning. This partitioning creates a lateral composition gradient which introduces lateral diffusion in order to redistribute the two components across the interface and to sustain growth. As a result, the eutectic phase transformation is influenced by mass transfer processes.

To investigate the effect of convection on a stepped interface, and compare the results with that obtained for a planar interface, a theoretical model was formulated. A steady well developed, laminar flow was introduced in front of the solid-liquid interface, normal to the growth direction of the lamellae. The velocity field generated due to the flow of melt over the steps was solved numerically. The velocity profile obtained was incorporated into the governing mass transfer equation, which was solved using finite difference techniques. The geometry of the plane and the stepped interface with the co-ordinate system used are shown in figure 1. Here α and β are the two cooperatively growing adjacent phases of the binary eutectic. Figure 1 shows the β phase protruding into the melt creating a stepped interface. Here S_α and S_β are the half widths of the two phases, λ is the lamellar spacing and κ is the height of the step.

2. GOVERNING EQUATIONS

In addition to diffusion, the convective mass transfer generated by the flow along the solid liquid interface must be taken into account. The general steady state mass transfer equation can be written as

$$D\nabla^2 C - \vec{U} \cdot \nabla C = 0 \tag{1}$$

where D is the diffusion coefficient of the solute, $\vec{U}$ is the velocity profile obtained after solving the flow field numerically and C is the composition of the melt, ahead of the growing interface. The following assumptions were made while formulating the theoretical model:

- The fluid flow and concentration fields in the melt are well developed; entrance and side effects are negligible.

- The composition of the liquid melt far from the solid liquid interface is the eutectic composition C_e.

- The growth of the lamellae occurs along the direction normal to the interface with a constant velocity V.

- There is no side growth of the protruding phase.

- In the direction normal to the x-y plane, i.e. the interface, and parallel to the lamellae the velocity and concentration are uniform.

- Far from the interface the fluid flow is parallel to the interface.

- The coordinate system travels along with the interface, so that the interface is assumed to be fixed with melt flowing into it at velocity V.

- The partial molar volumes of the two constituents are same and constant in all the phases.

The governing partial differential equation 1 applied to this model system, taking into account the above assumptions, can be further simplified as:

$$\frac{\partial^2 C}{\partial x^2} + \frac{\partial^2 C}{\partial y^2} - \frac{U_y}{D}\frac{\partial C}{\partial y} - \frac{U_x}{D}\frac{\partial C}{\partial x} = 0 \tag{2}$$

The fluid velocity U_y in the y direction, and the fluid velocity U_x in the x direction are calculated using a software package called FLUENT. FLUENT is a computer code created by Creare incorporated for simulating a wide range of fluid flow problems. It uses a finite difference numerical procedure to solve the Navier-Stokes equation. The domain to be investigated is divided into a finite number of cells and the partial differential equation is discretized over these units to produce a sequence of algebraic relations. An iterative scheme is then employed to solve for the equations and yield the velocity U_x and U_y at each point in the finite difference grid over the problem domain.

3. BOUNDARY CONDITIONS FOR THE VELOCITY FIELD

The boundary conditions used for solving the Navier-Stokes equation and computing the velocity of the melt at each grid point in the concentration field ahead of the solid liquid interface are as follows:

- Far from the interface the convection inducing velocity U_x is proportional to the distance from the interface. The far field condition is applied at a certain distance from the interface such that above this boundary the U_x increases as a constant gradient and the effect of the irregularity of the interface is not felt anymore. Calculations were performed for obtaining the velocity field when the far field condition was at a distance of λ. It was found that the irregularity at the interface, i.e. the steps, are capable of perturbing the velocity field till a distance of $3\lambda/4$ only.
  Hence the following boundary condition was arrived at:

  $U_x = U_e$ at $y = 3\lambda / 4$
  $U_y = -V$ at $y = 3\lambda / 4$
  $U_z = 0$

- There is a no slip condition along the interface. This condition can be mathematically represented in the following form.

$0 \le x \le S_\alpha$	$y = 0$	$U_x=0,\ U_y= -V$
$S_\alpha \le x \le (S_\alpha + 2S_\beta)$	$y = \kappa$	$U_x=0,\ U_y= -V$
$x = S_\alpha$ and $(S_\alpha + 2S_\beta) 0 \le y \le \kappa$		$U_x=0,\ U_y= -V$

- Due to the periodicity of the lamellar structure the velocity field is also periodic with the following condition:

  $U_{x=0} = U_{x=\lambda}$ for all y

4.   BOUNDARY   CONDITIONS   FOR   THE CONCENTRATION FIELD

The boundary conditions used for determining the solute concentration in the melt ahead of the solid liquid interface shown in figure 2 are as follows:

- The composition remains at the eutectic far from the interface.

$C = C_e$ at $y = \infty$

- Due to conservation of matter at the inteface, the solute rejected at the freezing interface is equal to the solute diffusing into the melt away from the interfae. This condition can be mathematically represented in the following form.
  For α phase,

$$D \left(\frac{\partial C}{\partial y}\right)_{y=0} = -V \left(C_l - C_s^{\alpha}\right) \tag{3}$$

For β phase, with the stepped interface,

$$D \left(\frac{\partial C}{\partial y}\right)_{y=\kappa} = -V \left(C_l - C_s^{\beta}\right) \tag{4}$$

- There is no side growth, i.e. along the side of the step there is no diffusion in the x direction,

$$\left(\frac{\partial C}{\partial x}\right)_{y=0 \ to \ \kappa} = 0 \tag{5}$$

- The concentration field is periodic owing to the periodicity of the lamellar structure,

$$C_{(x=0,y)} = C_{(x=\lambda,y)} = C_{(x=n\lambda,y)} \quad n = 1, 2, .. \tag{6}$$

5. NUMERICAL SCHEME

To solve the partial differential equation 2 mentioned above an explicit finite difference scheme was employed. The domain over which this equation needs to be descretized is shown in the figure 2. The first and second derivatives were expressed in terms of the three point central differences. In form of central differences, the second derivatives can be expressed in the following form:

$$\frac{\partial^2 C}{\partial x^2} = \frac{C_{i+1,j} - 2C_{i,j} + C_{i-1,j}}{(\Delta x)^2} \tag{7}$$

$$\frac{\partial^2 C}{\partial y^2} = \frac{C_{i,j+1} - 2C_{i,j} + C_{i,j-1}}{(\Delta y)^2} \tag{8}$$

In the form of central differences, the first derivatives can be expressed in the following form:

$$\frac{\partial C}{\partial x} = \frac{C_{i+1,j} - C_{i-1,j}}{2\Delta x} \tag{9}$$

$$\frac{\partial C}{\partial y} = \frac{C_{i,j+1} - C_{i,j-1}}{2\Delta y} \tag{10}$$

Substituting equations 7-10 into 2 we have

$$(\frac{C_{i+1,j} - 2C_{i,j} + C_{i-1,j}}{(\Delta x)^2}) + (\frac{C_{i,j+1} - 2C_{i,j} + C_{i,j-1}}{(\Delta y)^2})$$
$$- \frac{U_y}{D} (\frac{C_{i,j+1} - C_{i,j-1}}{(2\Delta y)}) - \frac{U_x}{D} (\frac{C_{i+1,j} - C_{i-1,j}}{(2\Delta x)}) = 0 \tag{11}$$

Assuming the grid spacing in the x and y directions to be equal, i.e. $\Delta x = \Delta y$, the equation 11 acquires the following form:

$$\frac{1}{(\Delta x)^2} [C_{i+1,j} + C_{i-1,j} + C_{i,j+1} + C_{i,j-1} - 4C_{i,j}]$$
$$- \frac{U_y}{2D\Delta x} [C_{i,j+1} - C_{i,j-1}] - \frac{U_x}{2D\Delta x} [C_{i+1,j} - C_{i-1,j}] = 0 \tag{12}$$

Multiply through out by $(\Delta x)^2$ and rearrange to give:

$$C_{i+1,j} [1 - \frac{U_x\Delta x}{2D}] + C_{i-1,j} [1 + \frac{U_x\Delta x}{2D}] +$$
$$C_{i,j+1} [1 - \frac{U_y\Delta x}{2D}] + C_{i,j-1} [1 + \frac{U_y\Delta x}{2D}] - 4C_{i,j} = 0 \tag{13}$$

For further simplification we substitute $y = (j-1) \Delta y = (j-1)\Delta x$ and rearrange the equation to obtain:

$$C_{i,j} - C_{i+1,j} [\frac{1}{4} - \frac{U_x\Delta x}{8D}] - C_{i-1,j} [\frac{1}{4} + \frac{U_x\Delta x}{8D}]$$
$$- C_{i,j+1} [\frac{1}{4} - \frac{U_y\Delta x}{8D}] - C_{i,j-1} [\frac{1}{4} + \frac{U_y\Delta x}{8D}] = 0 \tag{14}$$

An iterative procedure is employed to solve the equation. The algorithm is as follows:

$$C_{i,j}^{n+1} = \theta \left(C_{i+1,j}^{n} \left[\frac{1}{4} - \frac{U_x \Delta x}{8D}\right] + C_{i-1,j}^{n+1} \left[\frac{1}{4} + \frac{U_x \Delta x}{8D}\right] \right.$$
$$\left. + C_{i,j+1}^{n} \left[\frac{1}{4} - \frac{U_y \Delta x}{8D}\right] + C_{i,j-1}^{n+1} \left[\frac{1}{4} + \frac{U_y \Delta x}{8D}\right] \right) + (1 - \theta) \, C_{i,j}^{n} \qquad (15)$$

where n signifies the iteration number and θ is the successive over relaxation factor.

6. FINITE DIFFERENCE FORM OF THE BOUND-ARY CONDITIONS

- Far from the solidification interface the composition is at the eutectic i.e. C $=C_e$ at y $= \infty$. This being an infinite boundary condition cannot be used to carry out a finite difference analysis. However it is known that at a distance of the order of a lamellar spacing from the solidification interface the concentration perturbations disappear [5]. So this boundary condition was tried for increasing values of y i.e. the distance from the interface, until the solution was independent of the domain size. It was found in the initial computations that the computed average interface concentration with y=λ/2 differed by less than 1% with that computed with y=λ. Hence in the subsequent computations it is justifiable to assume that C $=C_e$ at y=λ /2.
In the finite difference mesh this boundary condition becomes:

For j = λ /2 , $C_{i,j}$ = C_e for all i

- The solute rejected at the interface is equal to the solute diffusing away from the inteface owing to the conservation of matter. Using three point forward difference approximation for the first derivative we can define the interface solute concentration as a function of the two points above it. Substituting the forward difference equations in the boundary conditions 3 and 4 we have:
For the α phase

$$D \left[\frac{-3C_{i,1} + 4C_{i,2} - C_{i,3}}{2\Delta x} \right] = V \, (C_{i,1} - C_s^\alpha) \tag{16}$$

For the β phase

$$D \left[\frac{-3C_{i,\kappa} + 4C_{i,\kappa+1} - C_{i,\kappa+2}}{2\Delta x} \right] = V \, (C_{i,\kappa} - C_s^\beta) \tag{17}$$

- The side boundary condition 5 for $0 < y < \kappa$ becomes:
For x = S_α,

$$C_{i,j} = [4 \, C_{i-1,j} - C_{i-2,j}] / 3 \qquad i = S_\alpha, \; j = 1 \; to \; \kappa \tag{18}$$

For x = $(S_\alpha + 2S_\beta)$

$$C_{i,j} = [4 \, C_{i+1,j} - C_{i+2,j}] / 3 \qquad i = S_\alpha + S_\beta, \; j = 1 \; to \; \kappa \tag{19}$$

C. PLANS

The concentration fields in front of the planar and stepped interface will be numerically computed using finite difference techniques. The concentration field obtained ahead of the stepped interface will be further studied by varying the following growth parameters:

- Growth Rate, V
- Lamellar Spacing, λ
- Diffusion coefficient, D
- Convective Velocity, U_e

The effect of convection on the solute concentration for various eutectic compositions will be investigated. In order to correlate the effect of convection to the lamellar spacing it is required to minimize the average interfacial undercooling ΔT. The concentration field obtained is to be converted to lamellar spacing by calculating the average composition of the interface and minimizing the total interfacial undercooling using the Jackson and Hunt supercooling criterion [5]. The influence of convection on the lamellar spacing will be investigated for a eutectic growing with a stepped interface and with a planar interface and a comparitive study of the two cases will be conducted. Calculations will be performed for different eutectic compositions.

REFERENCES

1. Baskaran, V., and Wilcox, W.R., J. Crystal Growth, 67 (1984) 343.

2. Eisa, G. F., "Effect of convection on the microstructure of MnBi-Bi eutectic solidified from melt,"Ph.D thesis, Clarkson University, Pots dam, NY (August 1987)

3. Chandrasekhar, S., "Effect of convection on the microstructure of MnBi-Bi euectic," Ph.D thesis, Clarkson University, Potsdam, NY (August 1987)

4. Caram, R., Chandrasekhar, S., and Wilcox, W.R., "Influence of convec tion on rod spacing of eutectics" submitted for publication (J. Crystal Growth)

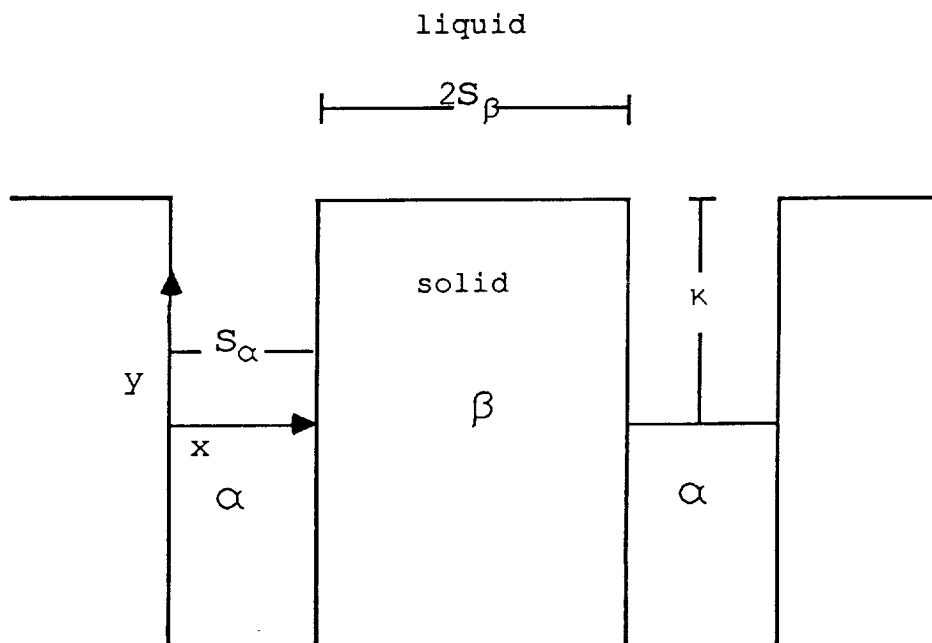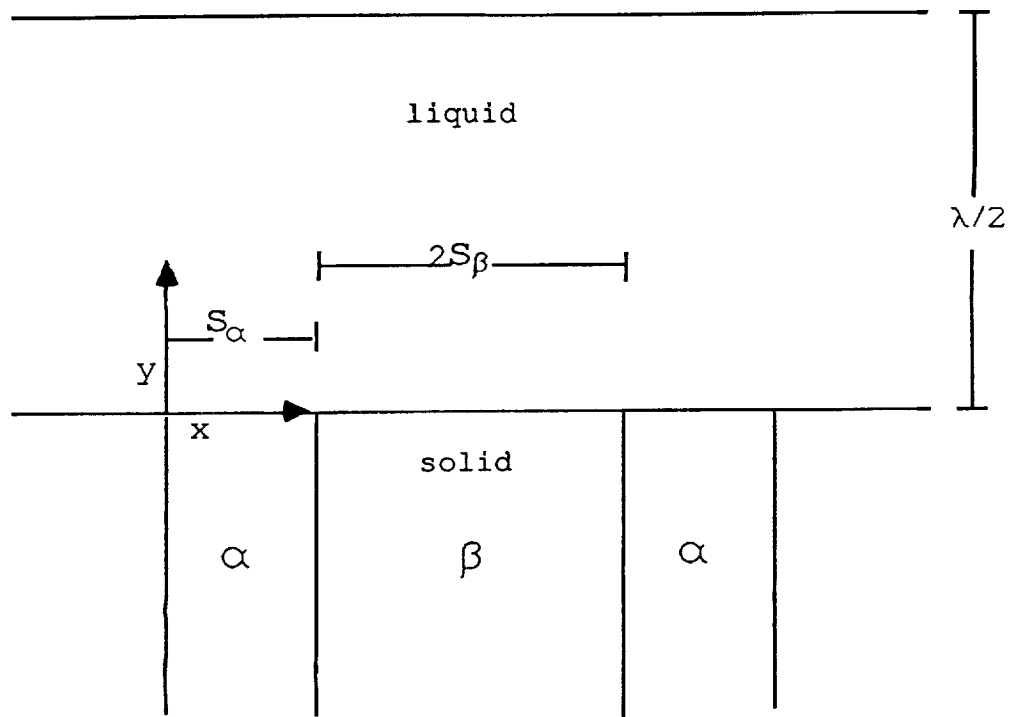5. Jackson, K. A., and Hunt, J . D., Trans, AIME 2368 (1966) 1129.

Figure 1: Schematic of the planar and stepped interface

$$C = C_e \text{ at } y = \lambda/2$$

$$C_{(x=0,y)} = C_{(x=\lambda,y)} = C_{(x=n\lambda,y)} \quad n = 1, 2, ..$$

$$D \left(\frac{\partial C}{\partial y}\right)_{y=0} = -V \left(C_l - C_s^\alpha\right)$$

$$\left(\frac{\partial C}{\partial x}\right)_{y=0 \ to \ \kappa} = 0$$

$$2S_\beta$$

$$D \left(\frac{\partial C}{\partial y}\right)_{y=\kappa} = -V \left(C_l - C_s^\beta\right)$$

κ

S_α

y
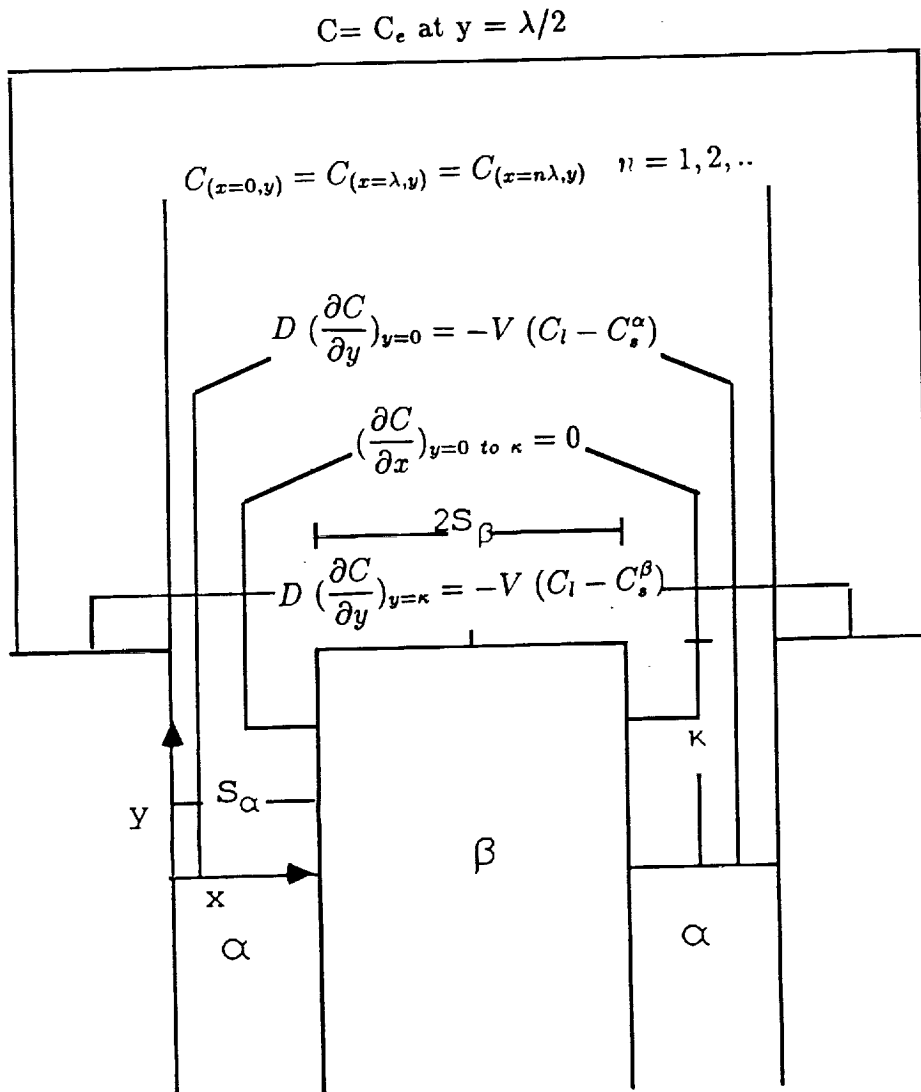
β

x

α

α

Figure 2: The boundary conditions for concentration field, for eutectic growing with a stepped interface